Journal of Renewable and Sustainable Energy

RESEARCH ARTICLE | FEBRUARY 15 2024

Photosynthetically active radiation separation model for high-latitude regions in agrivoltaic systems modeling

S. Ma Lu ; D. Yang ; M. C. Anderson ; S. Zainali ; B. Stridh ; A. Avelin ; P. E. Campana

Check for updates

J. Renewable Sustainable Energy 16, 013503 (2024)
https://doi.org/10.1063/5.0181311

View Online
Export Citation
CrossMark

06 March 2024 18:16:51

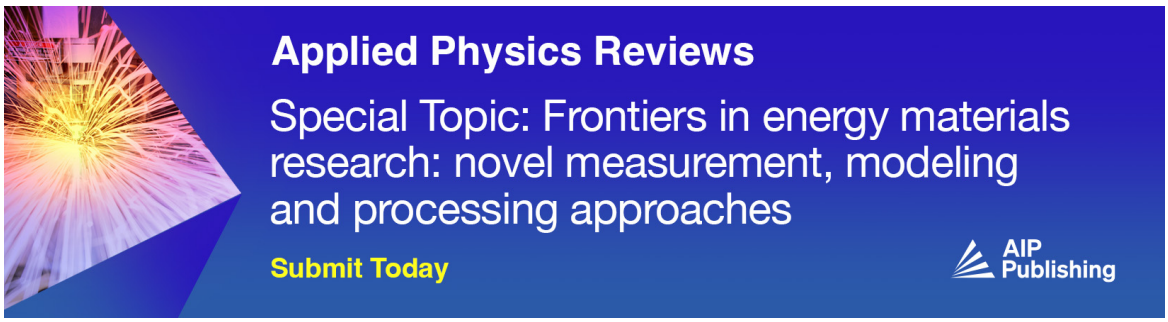

AIP Publishing

Journal of Renewable and Sustainable Energy ARTICLE pubs.aip.org/aip/rse

Photosynthetically active radiation separation model for high-latitude regions in agrivoltaic systems modeling

Cite as: J. Renewable Sustainable Energy **16**, 013503 (2024); doi: 10.1063/5.0181311
Submitted: 16 October 2023 · Accepted: 11 January 2024 ·
Published Online: 15 February 2024

View Online Export Citation CrossMark

S. Ma Lu,[1,a)] D. Yang,[2] M. C. Anderson,[3] S. Zainali,[1] B. Stridh,[1] A. Avelin,[1] and P. E. Campana[1,a)]

AFFILIATIONS

[1]Department of Sustainable Energy Systems, Mälardalen University, Västerås, Sweden
[2]School of Electrical Engineering and Automation, Harbin Institute of Technology, Harbin, Heilongjiang, China
[3]USDA ARS, Hydrology and Remote Sensing Laboratory, Beltsville, Maryland 20705, USA

[a)]**Authors to whom correspondence should be addressed:** silvia.ma.lu@mdu.se and pietro.campana@mdu.se

ABSTRACT

Photosynthetically active radiation is a key parameter for determining crop yield. Separating photosynthetically active radiation into direct and diffuse components is significant to agrivoltaic systems. The varying shading conditions caused by the solar panels produce a higher contribution of diffuse irradiance reaching the crops. This study introduces a new separation model capable of accurately estimating the diffuse component from the global photosynthetically active radiation and conveniently retrievable meteorological parameters. The model modifies one of the highest-performing separation models for broadband irradiance, namely, the YANG2 model. Four new predictors are added: atmospheric optical thickness, vapor pressure deficit, aerosol optical depth, and surface albedo. The proposed model has been calibrated, tested, and validated at three sites in Sweden with latitudes above 58 °N, outperforming four other models in all examined locations, with R^2 values greater than 0.90. The applicability of the developed model is demonstrated using data retrieved from Sweden's first agrivoltaic system. A variety of data availability cases representative of current and future agrivoltaic systems is tested. If on-site measurements of diffuse photosynthetically active radiation are not available, the model calibrated based on nearby stations can be a suitable first approximation, obtaining an R^2 of 0.89. Utilizing predictor values derived from satellite data is an alternative method, but the spatial resolution must be considered cautiously as the R^2 dropped to 0.73.

© 2024 Author(s). All article content, except where otherwise noted, is licensed under a Creative Commons Attribution (CC BY) license (http://creativecommons.org/licenses/by/4.0/). https://doi.org/10.1063/5.0181311

06 March 2024 18:16:51

I. INTRODUCTION

In land-based ecosystems, carbon uptake is primarily influenced by solar radiation during the daytime.[1] Photosynthetically active radiation (PAR) is the solar irradiance in the spectral interval between 400 and 700 nm.[2,3] PAR plays an essential role in plant photosynthesis and associated processes, such as greenhouse gas generation by the cultivation of crops (i.e., nitrous oxide) or biomass production.[4,5] The knowledge of PAR helps one to estimate the plant's primary production.[6] Like the global horizontal irradiance (GHI), PAR can also be partitioned into its diffuse $PAR_{diffuse}$ and direct PAR_{direct} horizontal components. This separation is of particular interest to many applications, especially for PAR estimation over land with complex topography, where the surrounding features can block the direct PAR component in an intricate and time-varying way.[7,8] Another application of this diffuse-direct separation of PAR is to study PAR distribution in plant canopies, where the diffuse light penetrates to a greater depth within the canopies than does the direct light.[9] Furthermore, the light-use efficiency of plant canopies increases under cloudy conditions due to the enhancement of the PAR diffuse component.[6,10,11] Li *et al.*[1] studied the influence of diffuse PAR radiation in a desert steppe ecosystem and concluded that the maximum canopy photosynthesis was reached under cloudy skies.

The implication of PAR separation becomes more profound in the field of agrivoltaic (APV) systems. The APV system is a novel concept that combines solar photovoltaic and agricultural activities on the same land area. APV technology is an efficient, effective, and innovative solution to tackling land use competition.[12] Nonetheless, one important concern of using such systems is that, for the coexistence of solar energy and agricultural farming, crop yield must not go below tolerable limits. It is known that shading generally decreases crop yield,

© Author(s) 2024

and different crops behave differently under shading conditions.[13] In open-field APV systems, the amount of PAR reaching the agricultural land is not homogeneously distributed. The solar modules installed in the system produce variable levels of shading directly on the crops throughout a day and over a year. In these shaded areas, the diffuse component of PAR plays a dominant role (Fig. 1). Therefore, knowing the amount of diffuse and direct PAR incident to a specific crop area beneath the APV system implies a more accurate crop yield estimation. Noticeably, the studies by Willockx *et al.*,[14] Campana *et al.*,[15] and Williams *et al.*[16] are among the first works in APV systems that introduced the concept of PAR separation for calculating ground light distribution and crop yield; the topic of concern is an exceedingly recent one. Other APV systems modeling studies have employed separation models of GHI, such as Orgill and Hollands[17] and Skartveit and Olseth,[18] to extract the ground light collection and used the full-spectrum global and diffuse solar radiation as input to crop models rather than global and diffuse PAR.[19,20]

Despite the relevance of PAR on crop growth, the scarcity of PAR measurements and the lack of a worldwide measurement network with standardized quality control (QC) protocols[21–23] directly explain the limited number of studies about PAR thus far as compared to, for example, the more extensive studies of GHI or diffuse horizontal irradiance (DHI).[24–26] The lack of measurements is even more pronounced for the diffuse component of PAR. Therefore, as a work-around, several authors have suggested a variety of models to estimate the various components of PAR. PAR components can be estimated using atmospheric radiative transfer models (ARTMs)[27–29] and methods derived from these (Refs. 30 and 31). However, since ARTMs can be highly complex and require extensive knowledge in the atmospheric sciences, most of the models used for applications in the field are empirical. These empirical models can derive the global component of PAR,[32] and a limited number can also derive diffuse PAR[33,34] from parameters commonly measured at weather stations[35–38] from spectral band measurement[39] and from satellite data.[40–42] The exhaustive review by Nwokolo *et al.*[43] offers an overview of empirical models to estimate the global horizontal PAR (i.e., $PAR_{global} = PAR_{diffuse} + PAR_{direct}$).

Several works have focused on the ratio global PAR/GHI and its behavior in different climate zones. According to the review by Noriega *et al.*,[44] the ratio is typically higher during summer and lower during winter, though exceptions to this rule have been highlighted by Yu and Guo[45] and Ma Lu *et al.*[46] Analysis of the global PAR/GHI ratio under cloudless conditions shows a clear dependence on air mass.[47] However, under all-sky conditions, the dependence of the ratio is unclear. Yu *et al.*,[48] Akitsu *et al.*,[49] and Ferrera-Cobos *et al.*[21] observed a decrease in the ratio when the clearness index (i.e., $k_t = GHI/E_{ext}$) increases. In contrast, Lozano *et al.*[50] found no significant dependence of the ratio on k_t. Most research studies admit that the global PAR/GHI ratio is location- and season-dependent,[37,51–53] therefore pointing out the need to further investigate the behavior of the ratio at more sites with different climates around the globe.

The $PAR_{diffuse}$ component is generally analyzed by the PAR diffuse fraction (i.e., $k_{PAR} = PAR_{diffuse}/PAR_{global}$). Several models have been proposed to obtain k_{PAR} and most of them are inspired by GHI separation models, which estimate DHI from GHI and their clearness index dependence.[34,54–57] Since the spectral range of PAR is a portion of that of GHI, it is logically attractive to just use GHI separation models to partition PAR_{global}. Indeed, the recent work by Ma Lu *et al.*[46] applied and evaluated several GHI separation models for separating PAR_{global}.

Generally, empirical models based on simple mathematical expressions reported in the literature are applicable when the local conditions are similar to those used for calibrating the models. However, a limited number of studies investigate the transferability of the models to other locations around the globe. For instance, de Blas *et al.*[58] analyzed the accuracy of 21 semi-empirical models of PAR_{global} in seven locations of the SURFRAD network in the United States that the authors claimed to be representative of a large variety of weather conditions. All 21 models use a combination of easily retrievable parameters. The results showed that refinement of the model parameters using local measurements can slightly improve local estimation of the PAR components. However, since the globally calibrated models (as opposed to locally calibrated ones) already offer very satisfactory results, they should be chosen considering the availability of the input variables at each specific location. However, the generalizability of these findings to northern European regions, like northern Germany and Scandinavia, where APV research has expanded in the last decade, is uncertain [59,60] given that the northernmost SURFRAD station used by de Blas et al.[58] was below <49 °N. To provide optimal performance at higher latitudes, the set of model predictors used may need to be tailored to the conditions specific to these regions, and different

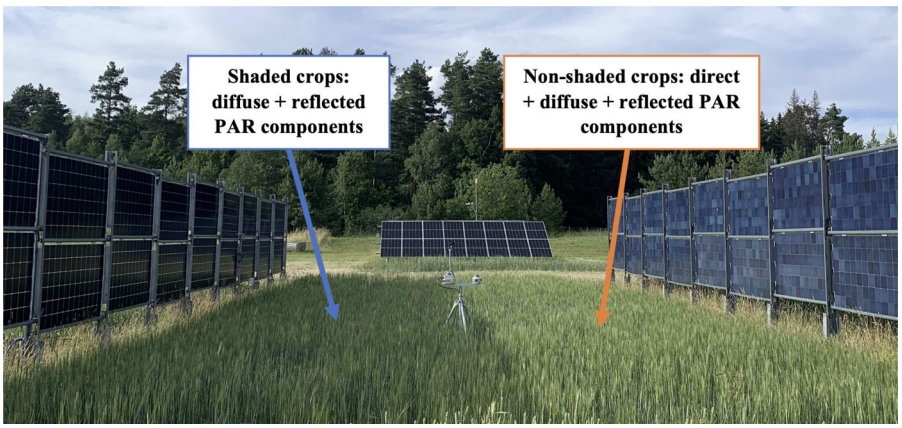

FIG. 1. Schematic of the photosynthetically active radiation components received at the crop level in shaded and non-shaded conditions in a vertical bifacial APV system located in Sweden.

06 March 2024 18:16:51

© Author(s) 2024

predictors may need to be considered. The correlation between PAR and meteorological variables is acknowledged to be location-dependent,[61] highlighting the need to scrutinize separation models developed with data from higher-latitude regions. López *et al.*[36] developed a model based on artificial neural network involving only GHI and solar zenith angle and compared it with an empirical model based on GHI, clearness index, and solar zenith angle[35] in Abisko, Sweden at latitude 68.35 °N; however, this model was for PAR_{global} estimation and not $PAR_{diffuse}$. Notably, a substantial knowledge gap persists regarding the transferability and performance of PAR separation models in high-latitude environments.

In the work presented here, a new separation model to estimate $PAR_{diffuse}$ from PAR_{global} is proposed. It is derived from the original YANG2 model,[62] which is a GHI separation model, because of its high accuracy demonstrated for both GHI and PAR_{global}.[46] In addition, the newly proposed model is based on atmospheric inputs conveniently retrievable from available databases, algorithms, and satellite-derived data. The proposed separation model is evaluated for three Integrated Carbon Observation System (ICOS) stations in Sweden, considering an evident gap in PAR separation model studies applied to northern latitudes exists and compared with the performance of four other PAR separation models. At the same time, an analysis of the seasonal trends and variation of the different PAR components is provided for these three locations.

Furthermore, the authors are currently conducting experiments on an APV system located near Västerås, Sweden. Three further evaluations, hereafter referred to as cases, of the proposed model are performed for this particular APV site. The primary objective of the first two study cases is to shed light on strategies for deriving the diffuse fraction of PAR using the proposed PAR separation model. This is particularly valuable for locations where *in situ* PAR measurements are unavailable, a common scenario. The third study case is aimed at offering guidance on when to employ a single-parameter separation model vs more intricate models. It is worth reiterating that the cases aim to illustrate the obtention of diffuse fraction of PAR, thus the diffuse PAR for a specific study location. The determination of diffuse PAR in an APV site serves as input for APV system modeling, much like how DHI functions in photovoltaic (PV) system modeling. They do not, however, intend to provide a detailed ground-level PAR distribution received by the crops within the APV system. This aspect falls outside the scope of our current work. For further information regarding the application of the PAR separation model to evaluate light distribution at the ground-level in the APV system modeling, the readers are kindly referred to Campana *et al.*[15]

The remainder of the study is organized as follows: Section II describes the steps taken to develop the new separation model and the methodology behind the studied cases. Section III presents the meteorological data used for developing, calibrating, testing, and validating the model proposed in this study as well as the data used from the APV site. More specifically, an analysis of the fluctuations in PAR components in these high-latitude locations is presented and discussed. Section IV evaluates the performance of the proposed model and discusses the results obtained for the selected sites. Additionally, the results of the three cases, showing different strategies to apply the proposed PAR separation model for APV system applications, are analyzed. Section V draws the conclusions of the study.

II. METHODOLOGY

The proposed PAR separation model is derived from the original GHI separation model YANG2,[62] which has been identified in previous work as the most accurate PAR separation model.[46] YANG2 itself is an adaptation of the Boland–Ridley–Lauret (BRL)[63] logistic form GHI separation model. As a result, the proposed model also follows the logistic form but incorporates additional predictors beyond those used in YANG2. These additional predictors have been carefully selected through a literature review, as presented in Sec. II A. Utilizing these new predictors, the new PAR separation model is constructed (Sec. II B), and the significance and coefficient estimates for these predictors are determined for the three ICOS stations via nonlinear regression (Sec. II C). To assess the performance of the proposed PAR separation model, four other existing PAR separation models are evaluated for the studied locations, and their results are compared using common statistical indicators for model assessment (Sec. II D). A graphical representation of the methodology is provided in Fig. 2.

Furthermore, the paper outlines three cases (Sec. II E) that demonstrate different strategies and applications of PAR separation models to obtain the diffuse PAR fraction in situations where $PAR_{diffuse}$ is not directly measured *in situ*. Such scenarios are common, but they have gained increased interest, especially for APV systems modeling as illustrated at the APV site near Västerås.

A. Literature review on the climatic parameters affecting the diffuse component of photosynthetically active radiation

An initial literature review has been performed to analyze which atmospheric variables most influence the ecosystem production efficiency and, thus, the PAR components.

In the study by Li *et al.*,[1] in a desert steppe ecosystem, lower vapor pressure deficit (VPD ≤ 1 kPa), lower air temperature (Ta < 20 °C), and non-stressed water conditions were more favorable conditions for enhanced ecosystem photosynthesis under cloudy skies ($k_t < 0.7$). $PAR_{diffuse}$ peaked when k_t was around 0.5.

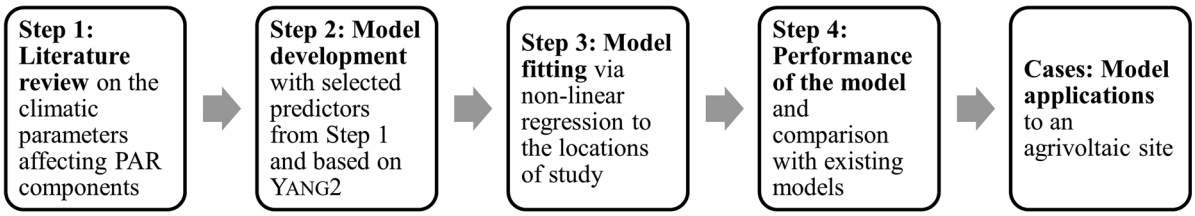

FIG. 2. Schematic diagram of the workflow applied in this work for the development of a new PAR separation model.

06 March 2024 18:16:51

© Author(s) 2024

A work by Lu *et al.*[64] using data from 40 sites around the globe has concluded that VPD and soil moisture (SM) are significant variables in ecosystem production efficiency that should be applied in ecosystem modeling. For most of the studied sites, high VPD values cause positive changes in PAR, while low SM values cause negative changes in the fraction of PAR absorbed by the plants (fPAR). The study underlines the influence of VPD on the incident PAR in a multitude of locations. Yet, none of those sites was in northern latitudes.

A new method to estimate PAR values for clear-sky conditions used solar zenith angle, total column contents of ozone and water vapor, aerosol optical depth (AOD), vertical profiles of temperature, pressure, density, and volume mixing ratio of gases, elevation, and ground albedo as inputs.[30] The study emphasized that the errors in the suggested method were caused by the overestimation of the input variables AOD and the assumption of constant PAR_{albedo}, suggesting that these two variables have a significant effect on the PAR under clear skies.

Recent work by de Blas *et al.*[58] analyzed PAR_{global} estimations at 1 min, hourly, and daily time steps at seven sites from 21 models that use a combination of the following meteorological parameters: GHI, clearness index, diffuse fraction, vapor pressure, relative optical air mass, precipitable water, solar zenith angle, sky brightness, and sky clearness. The work further analyzed the performance of the models for different groups of sky conditions (clear to overcast) and found that for some models, the accuracy worsened when applied to overcast skies.

Another recent work by Proutsos *et al.*[53] studied the atmospheric factors affecting the PAR/GHI ratio at a Mediterranean site. The authors concluded that the atmospheric water content (expressed by the degree of cloudiness, actual water vapor, optical thickness, or dew point temperature) and the clearness index were the most influential factors in the ratio. Air temperature and related meteorological variables (relative humidity, vapor pressure deficit, and saturation vapor pressure) were found to have no significant effect on the ratio.

Regarding PAR diffuse estimations, the latest work by Lozano *et al.*[50] found a clear dependence of the k_{PAR} on the clearness index and total cloud cover at a Mediterranean site. The authors proposed a model to estimate k_{PAR} obtained through the first adaptation of the BRL model[63] based on the PAR clearness index, solar elevation angle, apparent solar time (AST), daily PAR clearness index, and persistence index. When fitting the model to the studied site, the authors found that AST and daily PAR clearness index were insignificant and suggested these terms be removed from the model.

Kathilankal *et al.*[34] developed a semi-parametric PAR separation model for the United States. It adapts the BRL model using physically viable climate variables as predictors: relative humidity, PAR clearness index, surface albedo, and solar elevation angle. The proposed model takes a conditional approach, which uses two logistic fits: one for clear-sky conditions and the other for cloudy conditions.

Yamashita and Yoshimura[65] introduced a method for estimating global and diffuse PAR using whole-sky images captured with a commercial digital camera and fish-eye lens employing an equidistant projection. In their approach, they utilized these images to derive three sky condition factors, which were determined based on the ratios of cloud cover, Sun area, and brightness index. A fourth sky condition factor was incorporated by calculating the solar elevation angle. They developed models using these four sky condition factors to compute the clearness index, diffuse ratio, and quanta-to-energy global and diffuse variables, which were then used to estimate global and diffuse PAR. This novel method opens up the possibility of employing sky cameras for solar radiation assessment. However, it is important to note that obtaining these sky condition factors requires specific equipment, and if such equipment is unavailable, the necessary parameters must be collected using conventional sensors, algorithms, or satellite observations.

Based on the literature, the parameters VPD, AOD, optical thickness, relative humidity, and albedo are not included in the YANG2 model but appear to influence $PAR_{diffuse}$. In addition, their values can be retrieved with relative ease.

B. Model development

YANG2,[62] which is a logistic form model, has been selected as the starting point for developing the new PAR separation model. The logistic form is chosen based on the agreement in the literature as yielding higher accuracy for both separation models of GHI and separation models of PAR in comparison with other functional shapes. Previous work by Ma Lu *et al.*[46] showed that YANG2 and STARKE[66] were among the best-performing models to obtain $PAR_{diffuse}$ from PAR_{global}. It should be noted that both YANG2 [Eq. (1)] and STARKE [Eq. (4)] were originally developed for decomposing GHI by estimating the diffuse fraction, $k = \mathrm{DHI}/\mathrm{GHI}$. For this reason, Ma Lu *et al.*[46] have applied the Spitters relationship [Eq. (6)][67] to expand the applicability of these models to PAR separation

$$k^{\mathrm{YANG2}} = C + \frac{1-C}{1+e^{\beta_0+\beta_1 k_t+\beta_2 \mathrm{AST}+\beta_3 Z+\beta_4 \Delta k_{tc}+\beta_6 k^{(s)}}} + \beta_5 k_{de}, \tag{1}$$

$$\Delta k_{tc} = k_{tc} - k_t = \frac{G_{cs}}{\mathrm{E_{ext}}}, \tag{2}$$

$$k_{de} = \max\left(0, 1 - \frac{G_{cs}}{\mathrm{GHI}}\right), \tag{3}$$

$$k^{\mathrm{STARKE}} = \begin{cases} \dfrac{1}{1+e^{\beta_0+\beta_1 k_t+\beta_2 \mathrm{AST}+\beta_3 Z+\beta_4 K_T+\beta_5 \psi+\frac{\beta_6 G_{cs}}{277.78}}}, \\ k_{\mathrm{CSI}} \geq 1.05 \quad \text{and} \quad k_t > 0.65, \\ \dfrac{1}{1+e^{\beta_7+\beta_8 k_t+\beta_9 \mathrm{AST}+\beta_{10} Z+\beta_{11} K_T+\beta_{12} \psi+\frac{\beta_{13} G_{cs}}{277.78}}}, \\ \text{otherwise}, \end{cases} \tag{4}$$

$$K_T = \frac{\sum_{n=1}^{24} \mathrm{GHI}_n}{\sum_{n=1}^{24} \mathrm{E_{ext},n}}, \tag{5}$$

$$k_{\mathrm{PAR}}^{\mathrm{model}} = \frac{\mathrm{PAR_{diffuse}}}{\mathrm{PAR_{global}}} = \frac{\left[1+0.3\left(1-(k^{\mathrm{model}})^2\right)\right]k^{\mathrm{model}}}{1+\left(1-(k^{\mathrm{model}})^2\right)\cos^2(90-\beta)\cos^3\beta}. \tag{6}$$

Briefly, k_t is the clearness index, G_{cs} is the clear-sky GHI ($\mathrm{W/m^2}$), Z is the solar zenith angle (°), AST is the apparent solar time (h), $\mathrm{E_{ext}}$ is the extraterrestrial irradiance ($\mathrm{W/m^2}$), $k^{(s)}$ is the satellite-derived diffuse fraction, K_T is the daily clearness index, the ψ predictor is defined here as the three-point moving average of the clearness index, k_{CSI} is the clear-

06 March 2024 18:16:51

© Author(s) 2024

sky index calculated as the ratio of GHI to G_{cs}, and β is the solar elevation angle (°). To avoid repetition, the reader is directed to the original model's publications for a comprehensive explanation of the parameters' physical significance. C and $\beta_0, \ldots, \beta_{13}$ are the coefficients of the model. The superscript "model" in k^{model} and $k_{\text{PAR}}^{\text{model}}$ indicates the applicable separation model, for instance, YANG2 or STARKE.

In the present work, the model form of YANG2 is taken as a basis. The following model [Eq. (7)], hereafter called CLY (i.e., an abbreviation of the main developers' family names in alphabetical order), is proposed by including four new relevant variables, i.e., albedo, optical thickness, AOD, and VPD, derived from the literature review. The relative humidity was not considered due to its high correlation with VPD [Eqs. (10) and (11)]

$$k^{\text{CLY}} = C + \frac{1-C}{1+e^{\beta_0+\beta_1 k_t+\beta_2 \text{AST}+\beta_3 Z+\beta_4 \Delta k_{tc}+\beta_5 \alpha+\beta_6 \tau+\beta_7 \text{AOD}+\beta_8 \text{VPD}+\beta_{10} k^{(s)}}} + \beta_9 k_{de}, \tag{7}$$

$$\tau = ln\left(\frac{\text{E}_{\text{ext}}}{\text{BHI}}\right)\frac{1}{\text{AM}}, \tag{8}$$

$$\text{AM} = \frac{1}{\cos(Z) + 0.50572(6.07995 + (90 - Z))^{-1.6364}}, \tag{9}$$

$$\text{VPD} = e_s - e_a, \tag{10}$$

$$e_a = e_s \frac{\text{RH}}{100}, \tag{11}$$

$$e_s = 6.1078 \exp\left(\frac{17.27\text{Ta}}{\text{Ta} + 237.3}\right). \tag{12}$$

Here, α is the surface albedo, τ is the atmospheric optical thickness calculated according to the Beer–Lambert law,[68] BHI is the beam or the direct horizontal irradiance (W/m^2), AM is the air mass calculated using the definition by Kasten and Young,[69] AOD is the aerosol optical depth at 550 nm, VPD is the vapor pressure deposition (mbar), e_a is the actual vapor pressure (mbar), and e_s is the saturation vapor pressure (mbar), both calculated according to the Technical Committee on Standardization of Reference Evapotranspiration,[70] RH is the relative humidity (%), and Ta is the ambient temperature (°C). Similarly, C and $\beta_0, \ldots, \beta_{10}$ are the coefficients of the model.

To obtain the diffuse fraction of PAR using the proposed model, Eq. (6) should likewise be applied to Eq. (7). $k_{\text{PAR}}^{\text{CLY}}$ is obtained as follows:

$$k_{\text{PAR}}^{\text{CLY}} = \frac{\left[1 + 0.3(1 - (k^{\text{CLY}})^2)\right] k^{\text{CLY}}}{1 + (1 - (k^{\text{CLY}})^2)\cos^2(90 - \beta)\cos^3\beta}. \tag{13}$$

CLY is evaluated for the three selected ICOS network stations (described in Sec. III), and its performance is compared to that of the original YANG2 and STARKE models, in addition to two other PAR separation models mentioned in the literature review. These additional PAR separation models adapt the BRL logistic form model with distinct predictors and were developed to provide k_{PAR} without the need to implement the relationship outlined in Eq. (6). Kathilankal *et al.*[34] and Lozano *et al.*[50] proposed these models, hereafter called KATHILANKAL [Eq. (14)] and LOZANO [Eq. (16)], respectively, as follows:

$$k_{\text{PAR}}^{\text{KATHILANKAL}} = \begin{cases} \dfrac{1}{1+e^{-(\beta_0+\beta_1 k_{t\_\text{PAR}}+\beta_2 \text{RH}+\beta_3 \alpha+\beta_4 \sin(\beta))}}, \\ \quad k_{t\_\text{PAR}} \le 0.78, \\ \dfrac{1}{1+e^{-(\beta_5+\beta_6 k_{t\_\text{PAR}}+\beta_7 \text{RH}+\beta_8 \alpha+\beta_9 \sin(\beta))}}, \\ \quad k_{t\_\text{PAR}} > 0.78, \end{cases} \tag{14}$$

$$k_{t\_\text{PAR}} = \frac{\text{PAR}_{\text{global}}}{\text{PAR}_{\text{ext}}}, \tag{15}$$

$$k_{\text{PAR}}^{\text{LOZANO}} = \frac{1}{1+e^{\beta_0+\beta_1 k_{t\_\text{PAR}}+\beta_2 \beta+\beta_3 \text{AST}+\beta_4 K_{T\_\text{PAR}}+\beta_5 \psi_{\text{PAR}}}}, \tag{16}$$

$$K_{T\_\text{PAR}} = \frac{\sum_{n=1}^{24} \text{PAR}_{\text{global},n}}{\sum_{n=1}^{24} \text{PAR}_{\text{ext},n}}, \tag{17}$$

where k_{t_PAR} is the clearness index of PAR, K_{T_PAR} is the daily clearness index of PAR, and ψ_{PAR} is the persistence index defined here as the two-point moving average of the clearness index of PAR. Similarly, $\beta_0, \ldots, \beta_9$ are the coefficients of the models.

C. Model fitting

The coefficients of predictors for the proposed model CLY and four other models (YANG2, STARKE, KATHILANKAL, and LOZANO) are estimated using non-linear regression least squares fit with the MATLAB® R2023a built-in function *fitnlm*.[71] The choice of a least squares fit aligns with the statistical concept of consistency,[72] given that one of the primary evaluation metrics is the normalized root mean square error. Prior research on the calibration and evaluation of point forecasts has emphasized the concept of consistency.[73,74]

The algorithm for non-linear regression estimate model coefficients uses an iterative procedure beginning with initial values. The initial values for the four existing models are derived from the models' original publications, whereas the initial values for the proposed model are similar for the predictors appearing in the YANG2 model and 0 for the new predictors. The maximum number of permitted iterations and other parameters (such as tolerances) are left at their default values.[71]

D. Model evaluation metrics

The performance of the proposed CLY model [Eq. (7)] is evaluated by employing several popular error metrics. The results are compared to the performance of four other models described previously at the same studied locations.

The error metrics selected in this work are the same ones utilized by Ma Lu *et al.*,[46] the normalized mean bias error (nMBE), the normalized root mean square error (nRMSE), and the coefficient of determination (R^2). The observations of k_{PAR} are derived from the measurements of $\text{PAR}_{\text{global}}$ and $\text{PAR}_{\text{diffuse}}$ at the studied ICOS stations. The predictions are the $k_{\text{PAR}}^{\text{model}}$ calculated from the models (i.e., CLY, YANG2, STARKE, KATHILANKAL, and LOZANO).

E. Model application cases

Three different cases are considered for the application of the proposed PAR separation model in APV systems. Although these cases utilize the CLY model, the approaches are valid for any existing

06 March 2024 18:16:51

© Author(s) 2024

separation models provided that the required parameters and data are known.

In **case 1**, the APV system's location is known, but there are no *in situ* measurements nor nearby weather station data available to feed the model. The approach involves using input data solely from available satellite-derived databases for the proposed PAR separation model. The CLY model applied in this case is calibrated using the combined measured training data from the three studied ICOS network stations. The accuracy of this approach is then compared to *in situ* measurements of the diffuse fraction of PAR at the APV site, located near Västerås, Sweden. The required input data for the CLY model's predictors in this specific scenario are gathered as outlined in Table I.

In **case 2**, the proposed CLY model, calibrated using the combined measured data from the three Swedish ICOS network stations studied previously, is also applied to the APV site in Västerås. However, in this case, the input data required by the CLY model are assumed to be known (i.e., measured *in situ*) (Table I). Similarly, the accuracy of this second approach is compared to the *in situ* measurements of the diffuse fraction of PAR.

Case 3 follows a similar model validation approach as with the studied ICOS stations. It assumes that all the required data to run the model at the APV site are known, including the PAR diffuse for a specific period (Table I). The model is calibrated using 2/3 of the available measured data, which includes the *in situ* measurements of the diffuse fraction of PAR and then tested with the remaining unseen data (1/3 of the available measured data). The same testing data are also used with the Erbs single-parameter separation model[75] of GHI [Eq. (18)] with the Spitters relationship [Eq. (6)] to obtain the diffuse fraction of PAR. Erbs has been used in a previous APV study to determine the $PAR_{diffuse}$ component[14] and is also incorporated into PV modeling tools such as *pvlib*[76] and PVsyst® for obtaining the DHI from GHI. Additionally, the same testing data are used for the CLY model using the coefficients from the combined ICOS sites (as in case 1 and case 2). The performance of the CLY model calibrated to *in situ* measurements, CLY model calibrated to the three ICOS network stations, and the Erbs model are then compared using the same indicators as in Sec. II D. The objective of this comparison is to highlight that simple GHI separation models like Erbs can be directly applied to decompose PAR.[46] However, caution must be exercised as the value of the diffuse fraction of GHI does not necessarily equal the value of the diffuse fraction of PAR [the Spitters relationship, Eq. (6), should be considered]. Additionally, it is possible that the one-parameter Erbs model is overly simple and fails to accurately represent the true distribution of the data. Another goal is to illustrate the differences between using the calibrated CLY model, especially for the location under investigation or utilizing a broad calibration derived from other stations within the same country

$$k^{\mathrm{ERBS}} = \begin{cases} 1.0 - 0.09k_t, & k_t \leq 0.22, \\ 0.9511 - 0.1604k_t + 4.388k_t^2 \\ \quad -16.638k_t^3 + 12.336k_t^4, & 0.22 < k_t \leq 0.80, \\ 0.165, & k_t > 0.80. \end{cases} \tag{18}$$

Table I details the input data sources used for the CLY model in the various examined cases, as well as the primary analysis performed for the three ICOS network[77] stations. This table summarizes for the reader the data sources utilized for each analysis.

TABLE I. Datasets used to obtain the predictor values of the proposed PAR separation model (CLY) for each of the cases under study. The Main Analysis column refers to the data used for developing, training, and testing the proposed model in three distinct Swedish ICOS network stations. Cases 1–3 are the studies located in the agrivoltaic (APV) site close to Västerås, Sweden. Note that cases 2 and 3 share the same data sources; their differentiation lies in the specific CLY model applied. Case 2 applies the CLY model calibrated to the ICOS-Sweden stations, while case 3 applies the CLY model calibrated to the APV site. In bold are the variables where the sources of the table refer to.

Predictor (Sub-variables)[a]	Main Analysis (Lanna, Degerö, Norunda)	Case 1 (APV site)	Case 2 (APV site)	Case 3 (APV site)
k_t (**GHI**, E_{ext}[b])	ICOS[77]	CERES[80]	Own measurements Sec. III D	Own measurements Sec. III D
AST	As described in Sec. III B	As described in Sec. III B	As described in Sec. III B	As described in Sec. III B
Z	As described in Sec. III B	As described in Sec. III B	As described in Sec. III B	As described in Sec. III B
Δk_{tc} ($\boldsymbol{G_{cs}}$, E_{ext}, k_t)	CERES[80]	CERES[80]	CERES[80]	CERES[80]
α	ICOS[77c]	CERES[80]	Own measurements Sec. III D	Own measurements Sec. III D
τ (E_{ext}, **BHI**, AM[d])	CERES[80]	CERES[80]	Own measurements Sec. III D	Own measurements Sec. III D
AOD	CAMS-AOD[81e]	CERES[80]	CERES[80]	CERES[80]
VPD (**RH, Ta**)	ICOS[77]	ERA5[82f]	Own measurements Sec. III D	Own measurements Sec. III D
$k^{(s)}$ (**GHI**, **DHI**)	CERES[80]	CERES[80]	CERES[80]	CERES[80]
k_{de} ($\boldsymbol{G_{cs}}$, **GHI**)	Same as for k_t and Δk_{tc}	Same as for k_t and Δk_{tc}	Same as for k_t and Δk_{tc}	Same as for k_t and Δk_{tc}

[a]The sub-variables required to obtain the value of the predictor are between parentheses.
[b]E_{ext} is obtained as described in Sec. III B.
[c]Albedo is calculated from ICOS parameters as the ratio of the outgoing shortwave radiation/incoming shortwave radiation from a net radiometer. For Norunda station, the albedo trend was dubious, and the predictor was initially insignificant (p-value > 0.05) when calibrating the model. Hence, CERES-derived albedo was instead used for Norunda.
[d]AM is obtained as defined in Eq. (9).
[e]AOD 550 nm from the CAMS-AOD satellite-derived service provided by ECMWF has a time step of 3 h. A shape-preserving piecewise cubic interpolation is used to achieve hourly data.
[f]ERA5 dataset provides air temperature (Ta) and dew point temperature (Td). The actual vapor pressure (e_a) can be derived from Td similarly as saturation vapor pressure (e_s) from Ta [Eq. (12)], since RH and Td are related.[83]

06 March 2024 18:16:51

© Author(s) 2024

Finally, a potential drawback of the proposed model lies in its elevated number of predictors, consequently increasing data requirements. Although the primary analysis compares the model against top-performing models, some of which also demand sophisticated data, it is valuable for the community to assess its performance against a more basic method besides ERBS. The well-established five-parameter ENGERER2 model[78] [Eq. (19)], recognized as a top-performing GHI separation model by Gueymard and Ruiz-Arias[79]'s analysis, is chosen. Commonly used in benchmarking studies, ENGERER2 is applied to the three mentioned cases, akin to the CLY model. Including ENGERER2 in the benchmark serves the dual purpose of demonstrating the added value of incorporating more sophisticated data, such as satellite-derived products, through our CLY model. In essence, this aims to aid readers in forming judgments on whether the additional effort to obtain these predictors for the CLY model is warranted in higher latitude regions

$$k^{\text{ENGERER2}} = C + \frac{1-C}{1+e^{\beta_0+\beta_1 k_t+\beta_2 \text{AST}+\beta_3 Z+\beta_4 \Delta k_{tc}}} + \beta_5 k_{de}. \quad (19)$$

III. DATA

The dataset used in this work for training and testing the proposed PAR separation model consists of multiple-year measurements of $\text{PAR}_{\text{global}}$ and $\text{PAR}_{\text{diffuse}}$ among other variables from the ICOS network in Sweden.[77] ICOS is a European research infrastructure, formed as a collaboration of nationally operated measurement stations. ICOS ecosystem stations follow standard protocols and requirements for all measured parameters.[84] To qualify for an ICOS station, pyranometers to measure GHI must meet the specifications required for the "First Class" (ISO 9060:1990 classification) or "Good Quality" (WMO class). PAR quantum sensors to measure $\text{PAR}_{\text{global}}$ and $\text{PAR}_{\text{diffuse}}$ must meet the minimum requirements detailed in Carrara *et al.*[84] The diffuse component must use either have a tracking shading disk system or a multi-sensor instrument with complex shadow pattern. Three locations in Sweden with available measurements were selected; namely, Lanna, Degerö, and Norunda (Fig. 3). The dataset spans three years of data for each station with a time resolution of 30 min. Since the measurements of PAR from ICOS stations are in units of flux density as a quantum process (PPFD), a conversion factor[3] of $1\,\text{W/m}^2 \approx 4.57\,\mu\text{mol/m}^2/\text{s}$ is applied whenever required. The data for each location are divided into two subsets. On the one hand, the training set consists of two years of data (2016–2017), which is used to fit the separation model parameters for the site. On the other hand, the validation (or testing) set consists of the remaining one year of data (2018), which is used to test the fitted models with unseen data for the location of concern.

A. Photosynthetically active radiation components variation at northern latitudes

These data analyses seek to shed light on the behavior of PAR components in regions with higher latitudes. The seasonal trends and variations of $\text{PAR}_{\text{global}}$, $\text{PAR}_{\text{direct}}$, and $\text{PAR}_{\text{diffuse}}$ for the three ICOS stations under study are depicted in Fig. 4. The monthly distribution of $\text{PAR}_{\text{global}}$ shows a clear cycle, with maximum mean and median values around May and July for all locations and the lowest values during winter. This seasonality trend is similarly observed in other studies for the northern hemisphere, such as the study by Lozano *et al.*[50] in

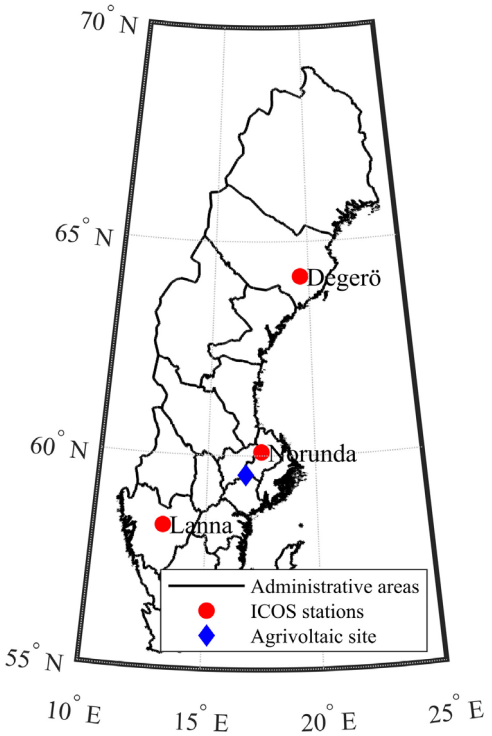

FIG. 3. Map of Sweden with the location of the ICOS Sweden network stations selected for the analysis and the location of the first agrivoltaic system in Sweden. Map source.[85]

Granada, Spain (37.16 °N, 3.61 °W). However, the magnitude of $\text{PAR}_{\text{global}}$ differs. In the Mediterranean location, the $\text{PAR}_{\text{global}}$ during the warmest months exhibited values higher than $250\,\text{W/m}^2$, while the maximum in the Scandinavian sites was around $150\,\text{W/m}^2$ (with the exception of 2018, which reached average values slightly below $200\,\text{W/m}^2$). Moreover, the Lanna station, located at the southernmost latitude, received on average 30.64% more annual $\text{PAR}_{\text{global}}$ radiation than Degerö, located 6° further north, for the period 2016–2017.

The seasonal pattern of the $\text{PAR}_{\text{direct}}$ component exhibits the highest variation and distribution. The direct component is clearly influenced by the Sun's position and the intensity of the incoming light. It is worth noting that 2016 and 2017 present similar distributions, while 2018 shows a significantly different distribution. The atypical behavior is aligned with the drought that occurred in Sweden in 2018. The country experienced an earlier onset of summer at the start of May, which lasted throughout the summer months, with short interruptions mainly in June.[86] For the three locations investigated, the average $\text{PAR}_{\text{direct}}$ value was 57.48% higher in May 2018 than in the previous two years. The increased solar irradiance in 2018 was caused by the anomalous presence of clear-sky conditions.[87,88]

The monthly variation observed in Fig. 4 for $\text{PAR}_{\text{diffuse}}$ is less pronounced than for $\text{PAR}_{\text{direct}}$ or $\text{PAR}_{\text{global}}$. The main reason is the high complexity of the scattering processes involved in the diffuse component, affected by the presence of clouds, aerosols, surface albedo, and altitude. For the investigated sites, the trend is similar for all the years with a slight alteration in 2018 due to a decreased amount of clouds,

06 March 2024 18:16:51

© Author(s) 2024

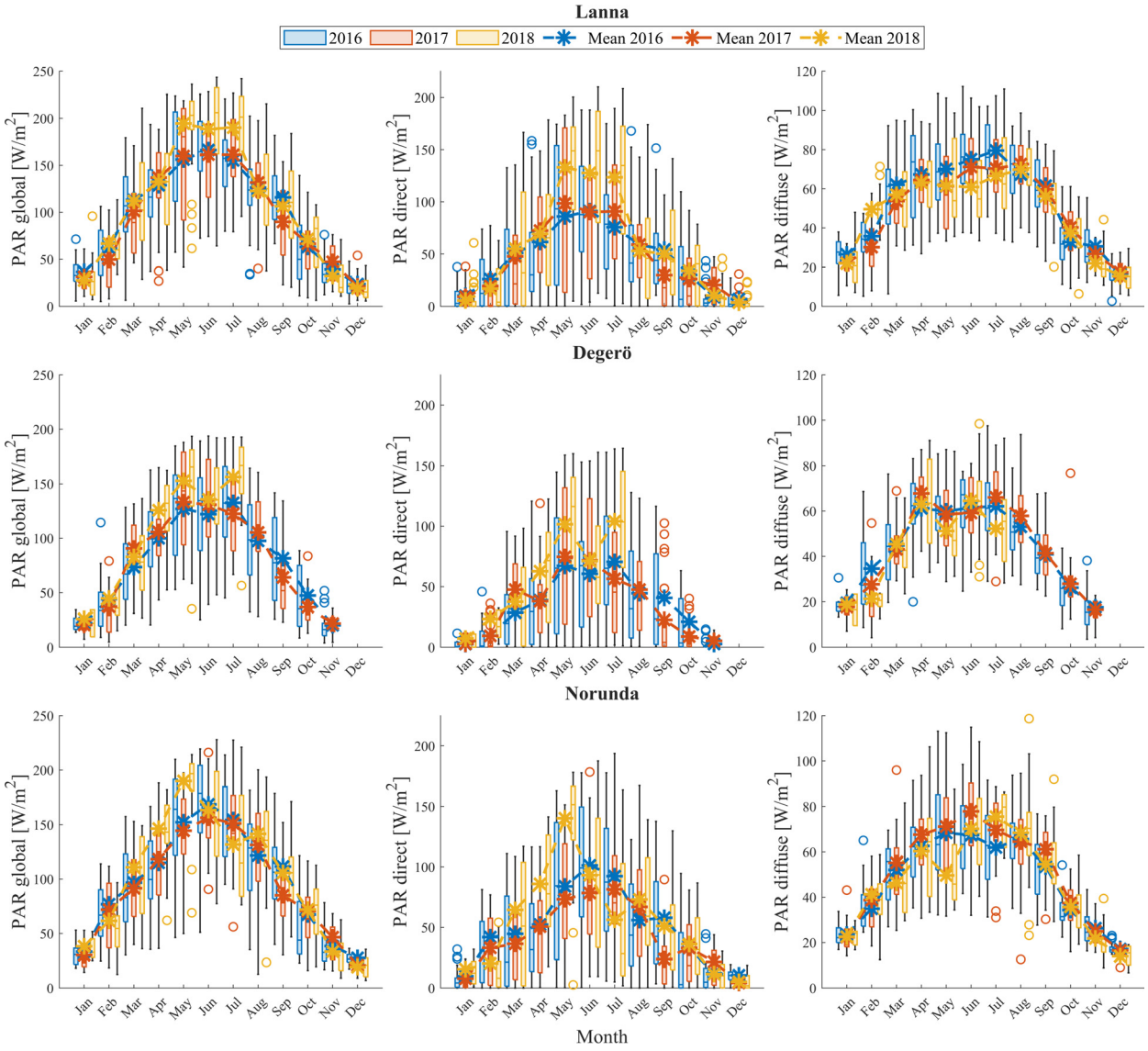

FIG. 4. Monthly variation box plots for PAR_{global}, PAR_{direct}, and $PAR_{diffuse}$ during the period 2016–2018 at the studied ICOS Sweden network stations: Lanna (top), Degerö (middle), and Norunda (bottom). For each box, central lines are the median, and upper and lower limits represent the percentiles 75th and 25th, respectively. The limits of the segments represent the minimum and the maximum daily average values. The circles represent outliers. The stars are the mean monthly values.

which brought overall lower values of $PAR_{diffuse}$. The annual mean $PAR_{diffuse}$ value for the locations studied was 46.65 W/m^2, marginally lower than the one reported by Lozano *et al.*[50] in Granada (Spain) 2008–2018 (59 W/m^2) and higher than the one reported by Trisolino *et al.*[89] in Lampedusa (Italy) 2002–2016 (35 W/m^2). Since there are scarce studies about PAR trends, the comparison is made to available studies in these Southern European locations. It is interesting to observe that the $PAR_{diffuse}$ is rather similar regardless of whether it is in the north or south of Europe.

Figure 5 presents the effect of cloudiness and atmospheric aerosols on PAR_{global}, PAR_{direct}, and $PAR_{diffuse}$ measurements for the investigated sites during the studied period. The upper envelope of PAR_{global} increases linearly with the clearness index. When the clearness index is low, $k_t < 0.3$, corresponding to thick cloud conditions,[90] $PAR_{diffuse}$ makes the primary contribution to PAR_{global}. $PAR_{diffuse}$ increases with increasing k_t, peaking at values of k_t around 0.5 under thin cloud conditions ($0.3 \leq k_t < 0.7$) and then decreases toward clear-sky conditions at high values of k_t. PAR_{direct} increases exponentially when the sky starts having clearer conditions ($k_t > 0.3$) and rapidly increases after the $PAR_{diffuse}$ decreases ($k_t > 0.7$). At high values, PAR_{direct} significantly contributes to the PAR_{global}. These trends are consistent across the three studied sites and align with Li *et al.*'s[1] findings in

06 March 2024 18:16:51

© Author(s) 2024

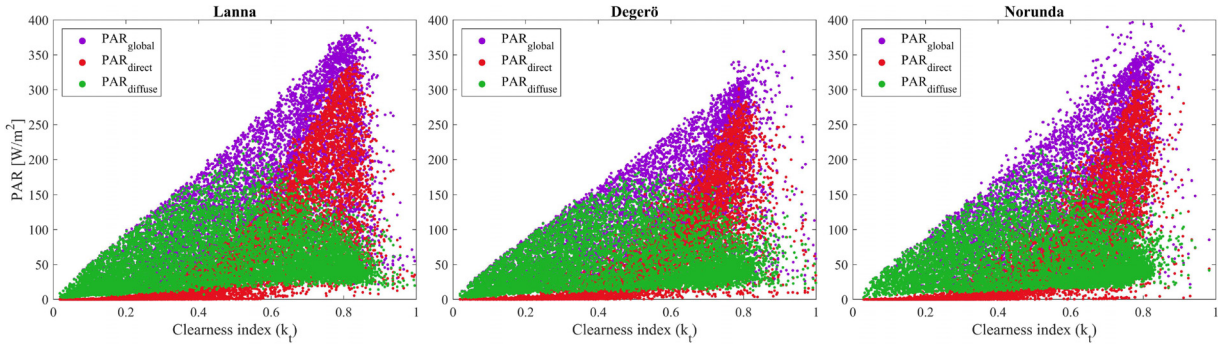

FIG. 5. Scatterplots between PAR_{global}, PAR_{direct}, and $PAR_{diffuse}$ and clearness index for the period 2016–2018 at the studied ICOS Sweden network stations: Lanna (left), Degerö (middle), and Norunda (right). Hourly values at midpoint are used.

a desert environment in the northern hemisphere. However, the magnitude of the PAR_{global} in this study is halved due to the climate and latitude characteristics.

The analysis demonstrates that the seasonality variation of PAR components and the relationship with cloudiness in high latitudes is similar to mid-latitudes in the northern hemisphere. However, the magnitude of the PAR components decreases as the location moves further north. This decrease is particularly noticeable for the PAR_{direct} component due to the distinct course of the solar zenith angle throughout the year resulting in reduced solar radiation. The $PAR_{diffuse}$ component, on the other hand, appears to have minor variability across seasons and locations, indicating that it is less influenced by the incoming solar irradiance and more likely to be affected by sky conditions and atmospheric aerosol content. It is important to highlight that this brief analysis covers three consecutive years for three stations. However, extended periods of data would be more advantageous to investigate the long-term trends and variability of PAR components comprehensively. Despite this limitation, the short-term analysis offers an initial glimpse into the characteristics of PAR components in high-latitude regions compared to other mid-latitude studies. It underscores the imperative need for PAR separation models tailored to the climate and latitude of these regions.

B. Auxiliary data

In addition to PAR_{global} and $PAR_{diffuse}$, separation models often require as input several auxiliary variables for training, which are often computable or can be accessed for general time periods and locations. These auxiliary variables are described in this section. First, the extraterrestrial irradiance (E_{ext}) on a horizontal plane is needed to compute k_t and is calculated as explained in Duffie and Beckman.[91] It is noted that the computation of E_{ext} requires further a parameter known as the solar constant (SC), which is here taken to be $SC = 1361.1\,W/m^2$, following Gueymard.[92] Moreover, the Earth's orbit eccentricity correction factor is used as per the definition by Spencer's equation.[93] From the eccentricity correction factor, the hour angle and thus the apparent solar time can be derived.[91] Extraterrestrial PAR (PAR_{ext}) is calculated analogously to E_{ext}, but with the approximated PAR solar constant, which is integrated from the latest synthetic extraterrestrial spectrum by Gueymard[92] between 400 and 700 nm, $PAR_{SC} = 531.8\,W/m^2$.

The solar zenith angle is calculated from the solar elevation, and the latter is derived using the solar positioning algorithm developed by Koblick.[94] Moreover, to account for the atmospheric refraction effects, the model from the ESRL Global Monitoring Laboratory[95] is applied to correct the solar elevation angle. The G_{cs} is acquired from the Clouds and the Earth's Radiant Energy System (CERES) satellite-based observations.[96] Both satellite-derived diffuse fraction of GHI and the diffuse fraction of PAR are obtained from the CERES SYN1deg Ed. 4.1 product.[80] CERES offers hourly satellite-derived GHI, DHI, PAR_{global}, and $PAR_{diffuse}$ from March 2000 till December 2022 with global coverage with a $1^\circ \times 1^\circ$ spatial resolution in both latitudes and longitudes. All satellite-derived data are downloaded via the ordering portal to match the spatial locations and the temporal range of the measured ICOS data.

It should be noted that even though ICOS data has a temporal resolution of 30 min (timestamp at the end of the averaging interval), due to the shortest time step availability of CERES data, which has an hourly resolution, the remaining part of this work (including both analysis and results) is performed with a 1 h time step Coordinated Universal Time (UTC). In the present study, the half-hourly data points from ICOS are averaged for hourly resolution. Solar zenith angle values are centered at the half of the hourly values. The metadata of the sites considered in this study is tabulated in Table II after quality control.

TABLE II. Study locations and details of the data extracted from the ICOS-Sweden network. The last column indicates the numbers of train/test samples (or data points) at each location after quality control and hourly resolution.

Station	Latitude (°N)	Longitude (°E)	Elevation (m)	Data period	Samples training/testing
Lanna	58°20′	13°06′	75	2016–2018	6638/3318
Degerö	64°18′	19°55′	270	2016–2018	6672/2003
Norunda	60°05′	17°29′	46	2016–2018	5671/2629

06 March 2024 18:16:51

© Author(s) 2024

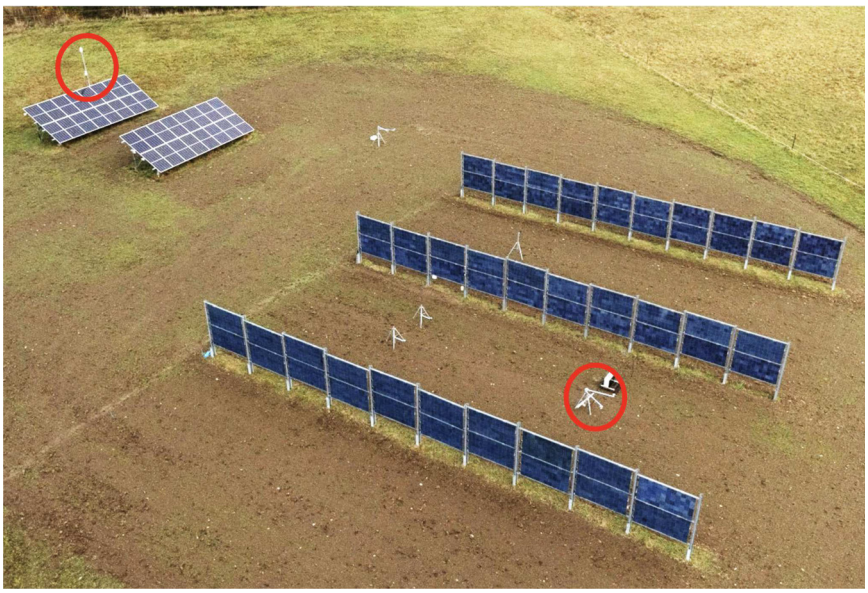

FIG. 6. Aerial picture of the first agrivoltaic system in Sweden comprising three vertical bifacial PV rows. The sensors measuring climatic parameters, solar irradiance, PAR irradiance, and albedo used in this study are situated in the red circles. Note that other sensors can be seen in the picture; however, these are not utilized for this particular study. Photo credit: Jonathan Lövholm, IVAR Studios AB.

C. Quality control

Quality control (QC) constitutes an essential part of radiation modeling, with the goal of filtering and eliminating spurious and erroneous data points. Since the observational data are to be used for the determination of fitting parameters, validation, and performance comparison of the separation models, QC must be applied to ensure that exclusively the highest-quality data points are selected. That said, there is no ideal or universally accepted QC procedure for broadband irradiance data, not to mention PAR data. This issue has been pointed out in the Introduction and in the previous work by Ma Lu *et al.*[46] The following quality checks have been applied:

1. $\mathrm{GHI} \leq 1.5\mathrm{E}_{\mathrm{extn}} \cos^{1.2}(Z) + 100$,[79] $\mathrm{E}_{\mathrm{extn}}$ is the extraterrestrial irradiance on a normal surface and calculated as explained in Duffie and Beckman.[91]
2. $\mathrm{GHI} \geq 5\,\mathrm{W/m^2}$, QC proposed by the European Commission's Daylight project.[34]
3. $Z < 85°$ to avoid cosine response issues.[79]
4. $\mathrm{PAR}_{\mathrm{global}} < \mathrm{PAR}_{\mathrm{ext}}$.[37]
5. $\mathrm{RH} < 100\%$, otherwise measurement accuracy might be affected by water droplets formed on the sensor.[34]
6. $0 \leq \alpha \leq 1$, albedo values between 0 and 1.
7. $0 \leq k_{\mathrm{PAR}} \leq 1$.

Those measured data points not respecting the above conditions were rejected and not considered for the analysis.

D. Agrivoltaic site data

The APV site under investigation is situated near Västerås (59.55 °N, 16.76 °E), Sweden. It comprises a vertical bifacial PV system of three rows. Additionally, there is a reference ground-mounted 30° fixed-tilt conventional PV system comprising two rows. The site is equipped with various monitoring devices to measure microclimatic parameters, as depicted in Fig. 6. However, for the purpose of this study, the sensors used are exclusively gathered from the reference station, positioned on a mast at a maximum height of 5 m above ground. This reference station captures the primary weather conditions of the site. Albedo data were collected from the middle of the vertical system (Fig. 6).

The dataset comprises *in situ* $\mathrm{PAR}_{\mathrm{global}}$ and $\mathrm{PAR}_{\mathrm{diffuse}}$ measurements taken from April to December 2022. These PAR measurements were recorded at a 1 min time resolution using a Delta T BF5 Sunshine Sensor, equipped with an array of photodiodes and a computer-generated shadow mask. The BF5 Sunshine Sensor does not need routine adjustment or polar alignment and does not have moving parts nor shade rings.[97] The hourly averaged PAR measurements are used to calculate the *in situ* k_{PAR}, which is then compared to the predicted k_{PAR} from the proposed model.

In the first case, all the input parameters required for the proposed model are derived from available databases, specifically CERES[80] and ERA5.[82] For the second and third cases, the input parameters used to feed the proposed model are based on a combination of *in situ* measurements and satellite-derived databases. The *in situ* measurements required as input data into the models were also recorded at a one minute resolution. However, for this study, these measurements have been aggregated to an hourly temporal resolution. GHI was acquired using a Delta T SPN1 Sunshine Pyranometer (classified as "Good Quality" per WMO standards). Air temperature and relative humidity data were collected from a Lufft WS600-UMB Smart Weather Sensor, along with albedo data from an Apogee SP-710-SS Albedometer (classified as "Second Class" ISO 9060:2018).

Fortunately, recalibration was not deemed necessary for any of the sensors, as all of them had been installed within the past two years. To ensure data quality, all *in situ* measurements and satellite-derived parameters were processed by averaging them to an hourly temporal resolution and conducting rigorous quality checks, as detailed in Subsection III C.

06 March 2024 18:16:51

© Author(s) 2024

IV. RESULTS AND DISCUSSION

A. CLY separation model performance

The proposed CLY separation model for estimating diffuse PAR is evaluated alongside four other models at the three ICOS network stations, using hourly analysis and evaluated with relevant performance metrics. These include YANG2, STARKE, KATHILANKAL, and LOZANO as described in the methodology. Table III presents the models' performance.

Before delving into the comparison of the models under investigation, readers may note a general decrease in performance for most models at the Degerö site, as evidenced by reduced R^2 and increased nRMSE values. This decline is attributed to the limited testing dataset at the site, comprising only the initial seven months of available data (see Fig. 4). Given that the training dataset spans two years, covering all seasons, it is reasonable to expect an impact on performance when assessing only a subset of months in the year.

An enhanced approach for predicting the diffuse fraction of PAR would involve the monthly calibration of the model, contingent upon sufficient monthly data availability. However, demonstrating the efficacy of this approach extends beyond the scope of the current study. As the focus is primarily on comparing the performances of various models and maintaining consistency with the other two stations under investigation, employing identical datasets for training and testing is considered a fair evaluation.

The CLY model demonstrates superior accuracy in terms of nRMSE and R^2 compared to the other investigated models across all locations. The additional predictors in the CLY model, namely, optical thickness, vapor pressure deficit, aerosol optical depth, and surface albedo, enable a more precise representation of the scattering processes in the atmosphere, compared to the other models. Particularly, the CLY model effectively captures the shape of the data envelope and the larger spread (i.e., data variability), as depicted in Fig. 7. On the other hand, separation models with fewer predictors (i.e., KATHILANKAL and LOZANO) exhibit thinner envelopes. This limits their ability to illustrate all possible combinations of k_{PAR} for the same k_t observed in the measured data. In other words, these models are less capable of explaining variations in the dependent variable, resulting in lower accuracy. Interestingly, the nMBE of LOZANO in Lanna is the lowest. This could be attributed to the metric's definition, which measures systematic bias and evaluates whether the model predictions tend to be consistently higher or lower on average. Consequently, the model's predictions might exhibit a lower average bias but may not perform as effectively in capturing data variability (Fig. 7), hence resulting in lower R^2 and nRMSE values.

Furthermore, the KATHILANKAL model, originally developed for the United States and based on data from several locations in the country (including one high-latitude location at 68.99 °N), exhibited increased errors for lower solar elevation angles (common at higher latitudes). This could explain the lower accuracy obtained for the KATHILANKAL model in this study when compared to the others. During the literature review, the authors of the LOZANO model discovered that when fitting the model to their studied site at a latitude of 37.16 °N, the predictors AST and K_{T_PAR} were deemed insignificant and proposed to remove them. However, this trend is not observed for the studied high-latitude locations, as the p-values obtained for these coefficients are indeed significant (Table IV). This highlights the importance of model calibration and the varying impact of predictors at different latitudes and climates.

In a previous study by Ma Lu *et al.*,[46] the performance of the YANG2 and STARKE models was found to be among the leading ones. The CLY model slightly outperforms these two in terms of nRMSE and R^2. These two metrics collectively assess the overall predictive accuracy, encompassing both bias and variability. Interestingly, the YANG2 model displays an improved nMBE compared to CLY. This suggests that CLY may have a higher likelihood of underestimating predictions on average (negative nMBE) but it excels in capturing the variance (random error). The model fitting yielded significant coefficients (p-value < 0.05) for all investigated locations (Table IV). This finding aligns with the observations during the literature review stage regarding the influence of the additional predictors on $PAR_{diffuse}$.

Upon closer examination of Fig. 7, it becomes evident that the STARKE and LOZANO models outperform CLY and YANG2 at low k_{PAR}. The concentration of k_{PAR} values below 0.2 coincides with elevated k_t values, indicative of clear-sky conditions.[66] A scrutiny of the STARKE and LOZANO models reveals a primary distinction in the smoothing factors—daily clearness index and persistence index—predictors absent in CLY and YANG2. This implies that the additional predictors of the clearness index, K_T and ψ, significantly contribute to a better understanding of the clear-sky conditions depicted in the plots. However, the reliance of these smoothing factors on future values of the clearness index limits the real-time implementation of STARKE and LOZANO models.[62]

The underperformance of the CLY model at low k_{PAR} values may have implications for agricultural applications. From a qualitative standpoint, clear-sky days in the summer typically result in total PAR irradiances well above the light-saturation point of crops, beyond which higher irradiance does not enhance plant productivity.[98] Conversely, clear-sky days in the winter generally exhibit decreased solar intensity, potentially falling below the light-compensation point—the minimum light required for a positive photosynthesis rate. Consequently, the mismatch in k_{PAR} estimations by the CLY model should have a limited impact on summer and winter seasons. However, the influence of diffuse light on clear-sky conditions during

TABLE III. The nRMSE (%), nMBE (%), and R^2 in predicted hourly diffuse PAR from the proposed PAR separation model, CLY, compared to other four models. Locally fitted coefficients (using training data over 2 years, period 2016–2017) and validated (using testing data over 1 year, period 2018) at three ICOS-Sweden stations (Lanna, Degerö, Norunda). The errors are computed between the predicted and measured hourly PAR diffuse fraction values. Boldface denotes the best-performing model in a row.

Station	CLY	YANG2	STARKE	KATHILANKAL	LOZANO
nRMSE (%)					
Lanna	**12.58**	13.25	14.31	24.33	16.28
Degerö	**18.23**	18.62	20.28	21.61	19.67
Norunda	**15.71**	16.27	17.42	20.44	17.00
nMBE (%)					
Lanna	−3.23	−1.97	−3.10	2.91	**−1.36**
Degerö	−1.10	**0.37**	−1.8	1.21	−2.56
Norunda	−2.35	−1.75	−2.93	**0.33**	−1.45
R^2					
Lanna	**0.94**	0.93	0.92	0.77	0.90
Degerö	**0.90**	0.89	0.87	0.85	0.88
Norunda	**0.92**	0.91	0.90	0.86	0.90

06 March 2024 18:16:51

© Author(s) 2024

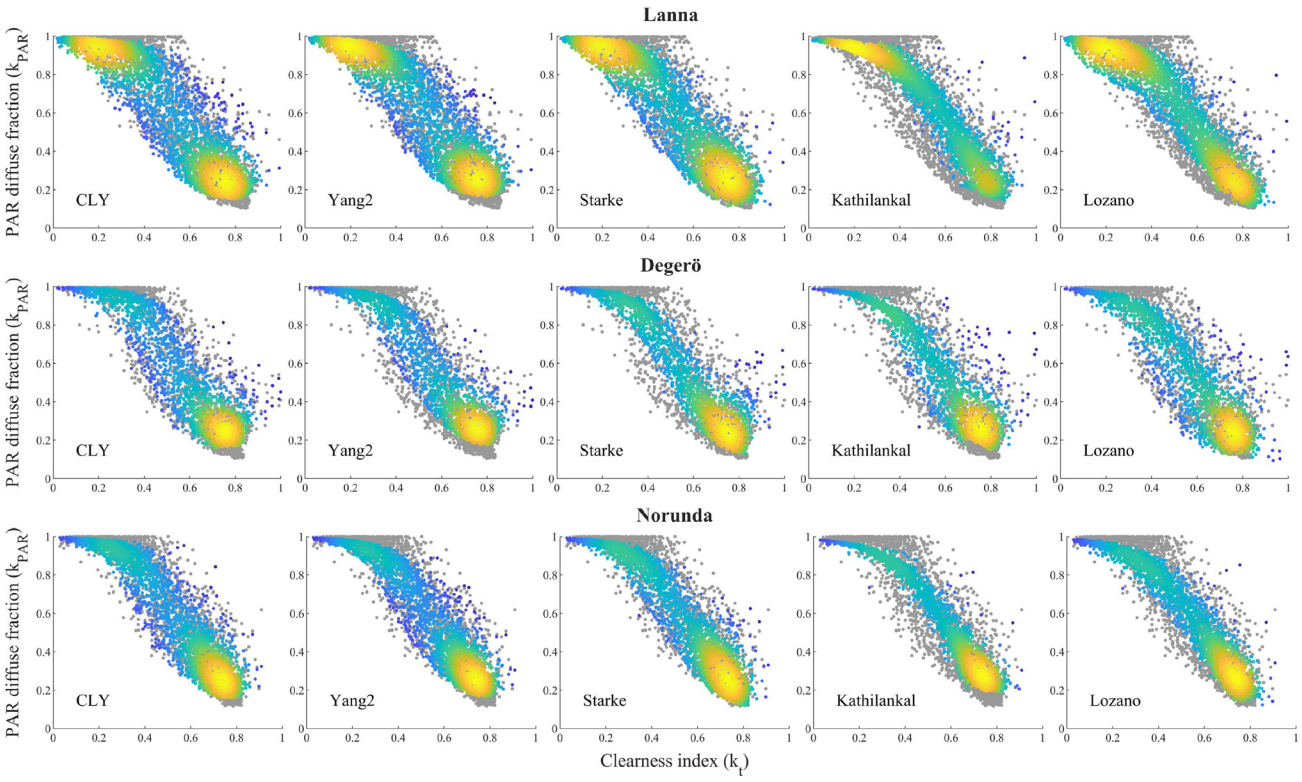

FIG. 7. PAR diffuse fraction measured data (gray dots) plotted against the clearness index for the studied locations: Lanna (top row), Degerö (middle row), and Norunda (bottom row). The estimated results from the proposed PAR separation model CLY, YANG2, STARKE, KATHILANKAL, and LOZANO are overlaid. The total number of data points in each plot refers to the testing data sample listed in Table II. Lighter colors indicate more points in the vicinity.

early and late crop growing seasons (e.g., spring and autumn) warrants further investigation. Understanding the impact of the CLY model's underperformance in these agricultural applications during specific periods could be an important focus for future studies.

Despite having several predictors, the proposed model is widely applicable thanks to the availability of satellite-derived data products (e.g., CERES,[80] MODIS,[99] CAMS[81]). However, it is essential to acknowledge that satellite-derived data have limitations in terms of both low spatial resolution and temporal resolution.[100] Therefore, when conducting site assessments for smaller areas or regions with diverse topography and significant variation in climate conditions, caution should be exercised when relying solely on satellite-derived data. The results obtained may reflect the average conditions of the entire pixel area covered by the satellite data, rather than the specific characteristics of the studied area. To ensure more accurate results, it is preferable to incorporate as many *in situ* measurements as possible as predictor values for the model.

B. Cases: Application of CLY separation model under different data availability

To showcase the versatility of the CLY PAR separation model and its applicability in diverse scenarios, three additional use cases are demonstrated on a site in Sweden with an actual APV system. It is worth reiterating that the utilization of the PAR separation model

TABLE IV. Model coefficients of the proposed CLY PAR separation model fitted via non-linear regression least squares method to the three ICOS stations in Sweden with hourly time step (Lanna, Degerö, and Norunda), each with 2 years of data corresponding to the period 2016–2017. In parentheses are the p-values.

Station	C	β_0	β_1	β_2	β_3	β_4	β_5	β_6	β_7	β_8	β_9	β_{10}
Lanna	0.1004	0.7564	4.7632	−0.1303	0.0032	−2.4211	−1.2458	−0.0712	−1.1196	0.0381	0.2390	−1.7076
	(0.000)	(0.000)	(0.000)	(0.000)	(0.016)	(0.000)	(0.000)	(0.001)	(0.000)	(0.000)	(0.000)	(0.000)
Degerö	0.1038	−1.8417	5.6991	−0.0469	0.0121	−2.1593	−0.5655	−0.1437	−0.6445	0.0622	0.7358	−1.4455
	(0.000)	(0.000)	(0.000)	(0.000)	(0.000)	(0.000)	(0.000)	(0.000)	(0.000)	(0.000)	(0.000)	(0.000)
Norunda	0.0841	−1.1836	5.6424	−0.0959	0.0075	−2.0551	−0.5010	−0.1674	−1.2362	0.0469	−1.0363	0.5121
	(0.000)	(0.000)	(0.000)	(0.000)	(0.000)	(0.000)	(0.037)	(0.000)	(0.000)	(0.000)	(0.000)	(0.000)

06 March 2024 18:16:51

© Author(s) 2024

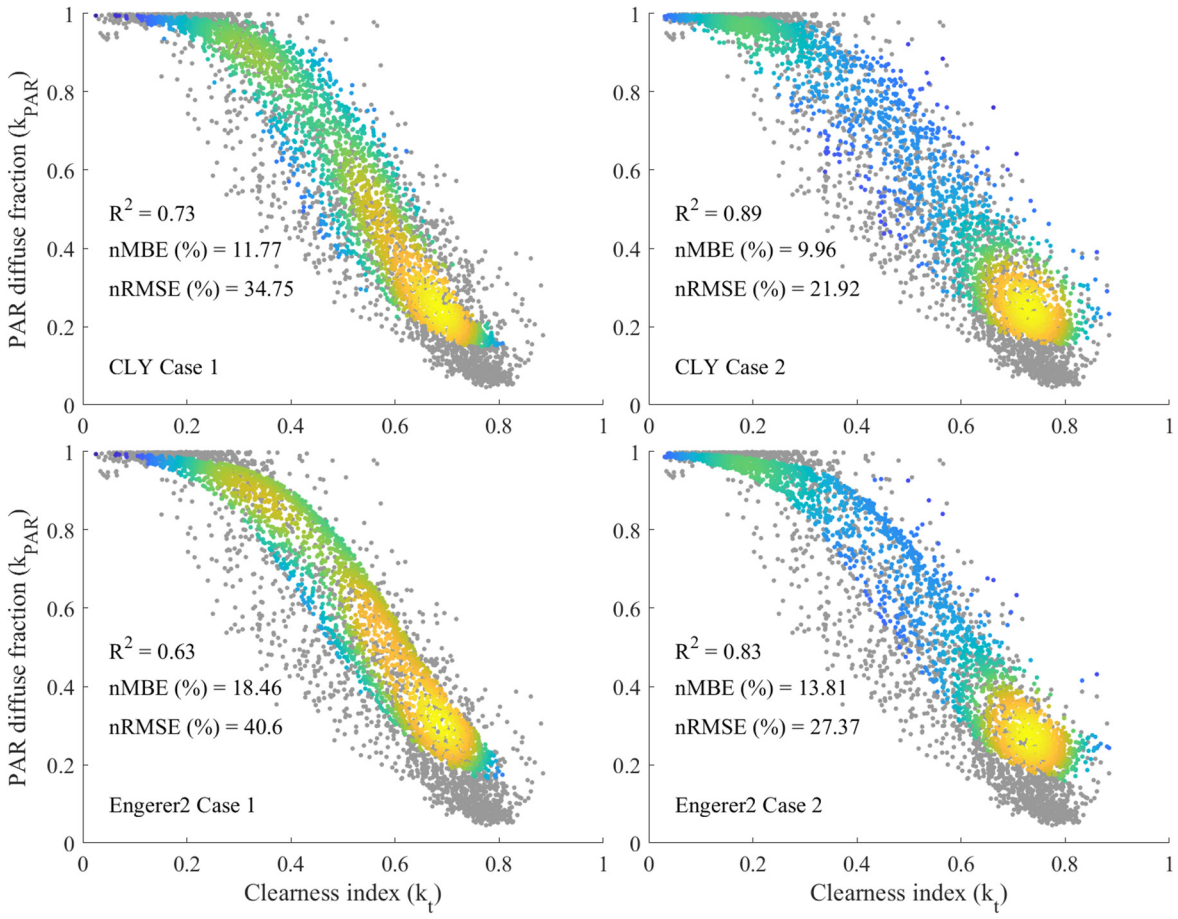

FIG. 8. PAR diffuse fraction measured data (gray dots) plotted against the clearness index for the agrivoltaic site near Västerås. The estimated results from the proposed PAR separation model CLY and ENGERER2 are overlaid. The total number of data points (2374) in each plot refers to the dataset described in Sec. III D and satellite-derived data after quality control. The nRMSE (%), nMBE (%), and R^2 are displayed. Lighter colors indicate more points in the vicinity. Left: results of case 1. Right: results of case 2.

represents an initial phase, allowing us to calculate the $PAR_{diffuse}$ and PAR_{direct} horizontal components at the site from PAR_{global}. To compute a comprehensive crop-level PAR distribution, it is essential to integrate algorithms that quantify the shading effects induced by the PV panels, such as the one described in Zainali *et al.*,[101] with the parameters derived from the PAR separation models.

1. Case 1

The results of the first case, where both the CLY and ENGERER2 separation models are exclusively applied with inputs collected from satellite-derived databases or derived algorithms, are presented in Fig. 8—left. Model coefficients are calibrated using combined data from the three ICOS network stations (Table V). The intention is to demonstrate the feasibility of calibrating the models using data from nearby stations that could represent the climate of the location under study. As expected, the accuracy of CLY is diminished compared to that achieved during model validation, primarily attributable to the lower spatial resolution of CERES satellite-derived observations.

The APV site covers a relatively compact area and is surrounded by forest and diverse vegetation within a radius of less than 1 km (Fig. 9). The CERES spatial resolution of 1° both latitude and longitude

TABLE V. Model coefficients of the proposed CLY PAR separation model fitted via the non-linear regression least squares method to: the combined three ICOS stations in Sweden with hourly time step (Lanna, Degerö, and Norunda) with 2 years of data corresponding to the period 2016–2017, and to the agrivoltaic site near Västerås with 2/3 of the data described in Sec. III D.

Station	C	β_0	β_1	β_2	β_3	β_4	β_5	β_6	β_7	β_8	β_9	β_{10}
ICOS combined	0.0946	−1.1230	5.6100	−0.0820	0.0084	−1.7992	−0.5080	−0.1209	−0.8215	0.0426	0.5262	−1.4605
Agrivoltaic site	0.0439	0.3510	6.2064	−0.0152	−0.0276	5.7983	−0.2302	−2.9454	1.6568	0.0254	0.4526	−1.2059

06 March 2024 18:16:51

© Author(s) 2024

indicates that input parameters from CERES are averaged to a grid size of ∼100 km^2,[102] resulting inevitably in the inclusion of varied environmental conditions that might not entirely mirror the conditions at the APV site. Despite this limitation, the results still present an acceptable initial approximation, with an nRMSE of 34.75% and an R^2 of 0.73 for this modest experimental APV site. It is noteworthy that accuracy could be enhanced for larger APV systems, covering a significantly larger area and potentially benefiting from improved spatial representation in satellite-derived data. When ENGERER2 is fed with CERES-derived GHI and clear-sky GHI data, the model also exhibits reduced performance owing to the constraints imposed by poor spatial resolution of CERES data.

2. Case 2

Similar to case 1, both the CLY model and the ENGERER2 model employed in this scenario have coefficients calibrated using combined data from the three ICOS network stations. However, in this case, the models receive input data directly measured from the specific APV site. The analysis period mirrors that of case 1, and the results are presented in Fig. 8—right. Compared to case 1, this second approach demonstrates higher accuracy, with CLY achieving an nRMSE of 21.92%. The second case enables a more precise estimation of k_{PAR}, and consequently, the $PAR_{diffuse}$ itself, as solar irradiance components, air temperature, and relative humidity are all measured *in situ*. This higher accuracy results from the availability of specific and reliable data acquired directly from the APV site, ensuring a faithful representation of its conditions. Similar to CLY, ENGERER2 also shows noticeable improvement compared to case 1.

3. Case 3

Ideally, an entire year of *in situ* measurements, spanning all seasons, would be available for model calibration. However, due to data limitations, a shorter period (April–December 2022) was utilized in this study. The CLY model, fitted to the APV site (Table V) and evaluated with the testing data, exhibits satisfactory performance (Fig. 10) akin to the outcomes from model evaluation.

To further compare this approach with case 2, the same testing data are used, and the results are displayed in Fig. 10. It is evident that the model with locally fitted coefficients outperforms the one calibrated to the ICOS network stations. Additionally, both the ENGERER2 and the ERBS model are also evaluated with the identical testing data, with results presented in Fig. 10. The single-parameter model ERBS proves inadequate in representing the data spread, resulting in both underestimation and overestimation of the observed k_{PAR}. The nMBE clearly indicates that when applying the ERBS model, predictions are generally overestimated by 10%, representing a significantly larger error compared to the CLY model. Although recalibrating ENGERER2 to the APV site enhances its performance, reducing the nMBE to −1.68%, it still falls behind the proposed CLY model.

4. Discussion

Different strategies for implementing the CLY PAR separation model, depending on data availability, have been demonstrated in an APV system within a high-latitude region. The following recommendations are suggested: in the absence of measured data, the CLY model

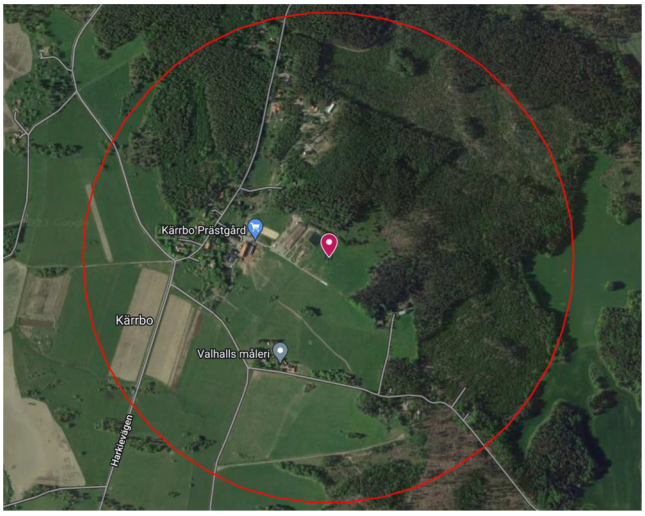

FIG. 9. Satellite image of the agrivoltaic site (red marker) near Västerås, Sweden. A red circle of radius 750 m with the agrivoltaic system in the center, illustrating the variety of terrain surrounding the site.[103]

can be calibrated using nearby stations with available data. Subsequently, satellite-derived data can be utilized as an initial substitute, particularly if the study site encompasses a large area with relatively uniform topography and vegetation. While the ERBS single-parameter model may yield satisfactory overall accuracy (nRMSE < 25% and $R^2 > 0.8$) by balancing positive and negative errors over time, it fails to capture the variability of k_{PAR} for the same value of k_t. To enhance the accuracy of k_{PAR} (nRMSE < 19% and $R^2 \geq 0.9$), the CLY model can be applied with coefficients calibrated to nearby stations where the required predictors are measured *in situ*. The highest accuracy is achieved when the model's output is locally known for a specific period, ideally spanning at least one year to encompass all seasons. This approach facilitates precise calibration of the model for the specific location, followed by feeding with *in situ* measurements for its predictors. To further benchmark the developed model, the well-known multi-parameter ENGERER2 model is evaluated as an alternative to the single-parameter ERBS model. Across all scenarios, ENGERER2 fails to surpass CLY. This appears to be consistent with Bright and Engerer's findings of ENGERER2's modest performance toward polar climates.[104] ENGERER2 or ERBS models may suffice for specific applications depending on data availability and accuracy requirements. The results presented enable readers to form their own judgment on whether gathering the necessary inputs for the CLY model is justified for their intended application.

V. CONCLUSION

The issue of conflicting land use between agricultural activities and ground-mounted solar photovoltaic power plants has become increasingly prevalent in recent years, and APV systems offer a potential solution to this problem. Accurately estimating $PAR_{diffuse}$ is crucial for analyzing APV systems, as crops situated underneath do not receive PAR_{global} in a uniform manner, as is the case in open-field conditions. Instead, they receive a non-uniform combination of $PAR_{diffuse}$ and PAR_{direct} due to the shading produced by the PV system, with

06 March 2024 18:16:51

© Author(s) 2024

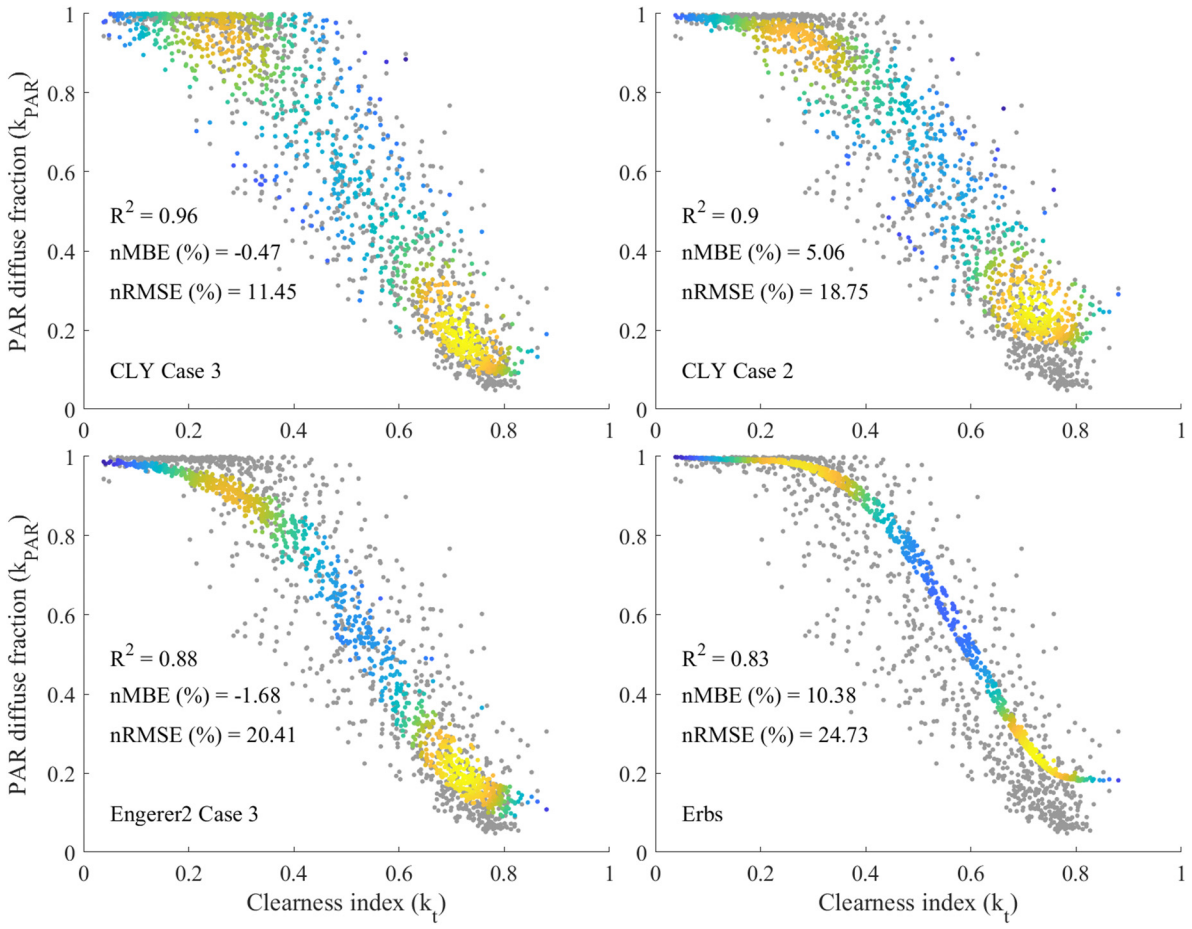

FIG. 10. PAR diffuse fraction measured data (gray dots) plotted against the clearness index for the agrivoltaic site close to Västerås. The estimated results from the proposed PAR separation model CLY, ENGERER2, and ERBS are overlaid. The total number of data points (994) in each plot refers to 1/3 of the dataset described in Sec. III D, where 2/3 of the dataset (1930 data points) are used for model calibration, both randomly split. The nRMSE (%), nMBE (%), and R^2 are displayed. Lighter colors indicate more points in the vicinity.

shaded areas receiving a greater proportion of $PAR_{diffuse}$. This shading typically reduces crop yields, making accurate calculation of $PAR_{diffuse}$ essential for more precise crop yield predictions.

To this end, the present study proposes a new separation model called CLY, which calculates $PAR_{diffuse}$ using the YANG2 decomposition model for GHI as a basis. The CLY model adds four additional predictors found relevant in previous studies, namely, ground albedo, optical thickness, vapor pressure deposition and aerosol optical depth.

The accuracy of the model has been compared to that of two previously identified best GHI separation models for PAR, namely, YANG2 and STARKE, and two purposefully developed PAR separation models, namely, KATHILANKAL and LOZANO, across different locations in Sweden. Results show that the CLY model outperforms all the compared models in all the studied locations. Across all locations, the model achieves R^2 values above 0.90, with an improvement between 1% and 17% in terms of R^2 when compared to the other studied models. Although the CLY model has only been validated in three locations at high northern latitude (>58 °N), primarily chosen because of the lack of studies in these regions, it could be subject to further studies to investigate its applicability and performance in other climates and at other temporal resolutions.

The developed PAR separation model was further applied to a site near Västerås, Sweden, where the country's first APV system is being investigated. Several cases were examined, considering different data availability scenarios. In cases where no *in situ* measurements are available, the results indicate that the CLY model can be calibrated using data from nearby stations. Subsequently, satellite-derived data can serve as a substitute, particularly if the site under study is vast and has uniform topography and vegetation. Even though ERBS single-parameter model, commonly used in PV simulation software to decompose GHI, cannot fully illustrate the variability of PAR diffuse fraction for the same value of k_t, its predictions tend to balance positive and negative errors over time, resulting in a satisfactory level of accuracy. To improve the estimation of the diffuse PAR fraction, the CLY PAR separation model can be employed with coefficients calibrated to nearby stations, provided the necessary predictors are measured *in situ*. Naturally, the greatest accuracy is achieved when the model's

06 March 2024 18:16:51

© Author(s) 2024

output is known for a specific period, preferable at least one year to account for all seasons. This allows for the precise calibration of the model at a particular location, as the model's predictors are based on measurements gathered on-site. Furthermore, ENGERER2 is benchmarked as a multi-parameter model with fewer predictors and reduced reliance on satellite-derived data, illustrating the enhanced accuracy that investing in the additional variables required for the CLY model can provide.

All the presented scenarios in this work were validated using *in situ* $PAR_{diffuse}$ measurements obtained above the canopy in an open-field reference environment (downwelling PAR radiation). Moving forward, the CLY PAR separation model will be integrated into the research group's APV integrated crop yield and PV power production model. The predictions of $PAR_{diffuse}$ will be spatially validated at the canopy level (i.e., ground level light distribution) in the APV system, accounting for the shading effects induced by the PV panels.

ACKNOWLEDGMENTS

The authors would like to acknowledge the financial support received from the Swedish Energy Agency through the project "The Solar Electricity Research Centre (SOLVE)" (Grant No. 52693-1). The author Pietro Elia Campana would like to acknowledge Formas—the Swedish Research Council for Sustainable Development—for the funding received through the early career project "Avoiding conflicts between the sustainable development goals through agro-photovoltaic systems" (Grant No. FR-2021/0005). The authors thank the Swedish Knowledge Foundation for the funding received through the project Optimized design of agrivoltaic systems in Sweden (Opti-APV) (Grant No. 20220032-H-01) co-founded by Linde Energi AB and Solkompaniet Sverige AB. The authors also acknowledge the Swedish Energy Agency for their financial support through the projects "Evaluation of the first agrivoltaic system in Sweden" (Grant No. 51000-1) and "Evaluation of the first agrivoltaic system facility in Sweden to compare commercially available agrivoltaic technologies—MATRIX" (Grant No. P2022-00809).

The authors would also like to acknowledge ICOS Sweden for providing the data from the Lanna, Degerö, and Norunda stations. ICOS Sweden is funded by the Swedish Research Council as a national research infrastructure. The authors also acknowledge the GEO Earth Observations for the water–food–energy nexus Community of Practice whose activities led to this paper. Finally, the authors would like to thank Dejwakh Kathleen for her assistance in better understanding the satellite-derived data obtained from the NASA Langley Research Center CERES ordering tool at https://ceres.larc.nasa.gov/data/.

AUTHOR DECLARATIONS

Conflict of Interest

The authors have no conflicts to disclose.

Author Contributions

Silvia Ma Lu: Conceptualization (equal); Data curation (lead); Formal analysis (lead); Methodology (lead); Validation (lead); Visualization (lead); Writing – original draft (lead); Writing – review & editing (equal). **Dazhi Yang:** Writing – review & editing (equal). **Martha Anderson:** Writing – review & editing (equal). **Sebastian Zainali:** Writing – review & editing (supporting). **Bengt Stridh:** Funding acquisition (lead); Writing – review & editing (supporting). **Anders Avelin:** Writing – review & editing (supporting). **Pietro Campana:** Conceptualization (equal); Funding acquisition (lead); Methodology (supporting); Writing – review & editing (equal).

DATA AVAILABILITY

The data that support the findings of this study are available in ICOS Data Portal (https://data.icos-cp.eu/portal/) and upon reasonable request from the corresponding author.

NOMENCLATURE

AM	Air mass
AOD	Aerosol optical depth
APV	Agrivoltaic
ARTM	Atmospheric radiative transfer model
AST	Apparent solar time
BRL	Boland–Ridley–Lauret model
CAMS	Copernicus atmosphere monitoring service
CERES	Clouds and the Earth's radiant energy systems
DHI	Diffuse horizontal irradiance
E_{ext}	Extraterrestrial irradiance on a horizontal plane
E_{extn}	Extraterrestrial irradiance on a normal surface
e_a	Vapor pressure (actual)
e_s	Vapor pressure (saturation)
fPAR	Fraction of PAR absorbed by plants
G_{cs}	Clear-sky global horizontal irradiance
GHI	Global horizontal irradiance
ICOS	Integrated carbon observation system
K_{T_PAR}	Daily clearness index of PAR
k_{t_PAR}	Clearness index of PAR
K_T	Daily clearness index
k	Diffuse fraction
k_{CSI}	Clear-sky global horizontal irradiance
k_{day}	Daily average of clearness index
k_{PAR}	Diffuse fraction of PAR
k_t	Clearness index
MODIS	Modern resolution imaging spectroradiometer
nMBE	Normalized mean bias error
nRMSE	Normalized root mean square error
PAR_{ext}	Extraterrestrial PAR on a horizontal plane
PAR	Photosynthetically active radiation
PPFD	Photosynthetic photon flux density
PV	Photovoltaic
QC	Quality control
R^2	Coefficient of determination
RH	Relative humidity
SM	Soil moisture
Ta	Temperature of air
Td	Dew point temperature
UTC	Coordinated Universal Time
VPD	Vapor pressure deficit
Z	Solar zenith angle

06 March 2024 18:16:51

© Author(s) 2024

α	Albedo
β	Solar elevation angle
τ	Optical thickness of the atmosphere
ψ	Clearness index persistence
ψ_{PAR}	Clearness index persistence of PAR

REFERENCES

[1]C. Li, X. Jia, J. Ma, P. Liu, R. Yang, Y. Bai, M. Hayat, J. Liu, and T. Zha, "Linking diffuse radiation and ecosystem productivity of a desert steppe ecosystem," PeerJ **8**, e9043 (2020).

[2]K. McCree, "Test of current definitions of photosynthetically active radiation against leaf photosynthesis data," Agric. Meteorol. **10**, 443–453 (1972).

[3]K. McCree, "The action spectrum, absorptance and quantum yield of photosynthesis in crop plants," Agric. Meteorol. **9**, 191–216 (1971).

[4]B. J. Keane, P. Ineson, H. W. Vallack, E. Blei, M. Bentley, S. Howarth, N. P. McNamara, R. L. Rowe, M. Williams, and S. Toet, "Greenhouse gas emissions from the energy crop oilseed rape (*Brassica napus*); the role of photosynthetically active radiation in diurnal N_2O flux variation," GCB Bioenergy **10**, 306–319 (2018).

[5]C. Tan, D. Wang, J. Zhou, Y. Du, M. Luo, Y. Zhang, and W. Guo, "Remotely assessing fraction of photosynthetically active radiation (FPAR) for wheat canopies based on hyperspectral vegetation indexes," Front. Plant Sci. **9**, 776 (2018).

[6]L. M. Mercado, N. Bellouin, S. Sitch, O. Boucher, C. Huntingford, M. Wild, and P. M. Cox, "Impact of changes in diffuse radiation on the global land carbon sink," Nature **458**(7241), 1014–1017 (2009).

[7]J. Olseth, "Spatial distribution of photosynthetically active radiation over complex topography," Agric. Meteorol. **86**, 205–214 (1997).

[8]Q. Wang, J. Tenhunen, M. Schmidt, O. Kolcun, M. Droesler, and M. Reichstein, "Estimation of total, direct and diffuse PAR under clear skies in complex alpine terrain of the National Park Berchtesgaden, Germany," Ecol. Modell. **196**(1-2), 149–162 (2006).

[9]M. Mariscal, S. Martens, S. Ustin, J. Chen, S. Weiss, and D. Roberts, "Light-transmission profiles in an old-growth forest canopy: simulations of photosynthetically active radiation by using spatially explicit radiative transfer models," Ecosystems **7**, 454 (2004).

[10]L. Gu, D. Baldocchi, S. B. Verma, T. A. Black, T. Vesala, E. M. Falge, and P. R. Dowty, "Advantages of diffuse radiation for terrestrial ecosystem productivity," J. Geophys. Res. **107**(D6), ACL 2-1, https://doi.org/10.1029/2001JD001242 (2002)

[11]K. D. Kanniah, J. Beringer, P. North, and L. Hutley, "Control of atmospheric particles on diffuse radiation and terrestrial plant productivity: A review," Prog. Phys. Geogr.: Earth Environ. **36**, 209–237 (2012).

[12]E. H. Adeh, S. P. Good, M. Calaf, and C. W. Higgins, "Solar PV power potential is greatest over croplands," Sci. Rep. **9**, 11442 (2019).

[13]G. A. Barron-Gafford, M. A. Pavao-Zuckerman, R. L. Minor, L. F. Sutter, I. Barnett-Moreno, D. T. Blackett, M. Thompson, K. Dimond, A. K. Gerlak, G. P. Nabhan, and J. E. Macknick, "Agrivoltaics provide mutual benefits across the food-energy-water nexus in drylands," Nat. Sustainability **2**, 848–855 (2019).

[14]B. Willockx, B. Herteleer, and J. Cappelle, "Combining photovoltaic modules and food crops: First agrivoltaic prototype in Belgium," Renewable Energy Power Qual. J. **18**, 266–271 (2020).

[15]P. E. Campana, B. Stridh, S. Amaducci, and M. Colauzzi, "Optimisation of vertically mounted agrivoltaic systems," J. Cleaner Prod. **325**, 129091 (2021).

[16]H. J. Williams, K. Hashad, H. Wang, and K. Max Zhang, "The potential for agrivoltaics to enhance solar farm cooling," Appl. Energy **332**, 120478 (2023).

[17]J. Orgill and K. Hollands, "Correlation equation for hourly diffuse radiation on a horizontal surface," Sol. Energy **19**, 357–359 (1977).

[18]A. Skartveit and J. A. Olseth, "A model for the diffuse fraction of hourly global radiation," Sol. Energy **38**, 271–274 (1987).

[19]M. Sojib Ahmed, M. Rezwan Khan, A. Haque, and M. Ryyan Khan, "Agrivoltaics analysis in a techno-economic framework: Understanding why agrivoltaics on rice will always be profitable," Appl. Energy **323**, 119560 (2022).

[20]B. Valle, T. Simonneau, F. Sourd, P. Pechier, P. Hamard, T. Frisson, M. Ryckewaert, and A. Christophe, "Increasing the total productivity of a land by combining mobile photovoltaic panels and food crops," Appl. Energy **206**, 1495–1507 (2017).

[21]F. Ferrera-Cobos, J. M. Vindel, R. X. Valenzuela, and J. A. González, "Analysis of spatial and temporal variability of the PAR/GHI ratio and PAR modeling based on two satellite estimates," Remote Sens. **12**(8), 1262 (2020).

[22]Y. Mizoguchi, Y. Ohtani, T. Aoshima, A. Hirakata, S. Yuta, S. Takanashi, H. Iwata, and Y. Nakai, "Comparison of the characteristics of five quantum sensors," Bull. FFPRI **9**, 113–120 (2010).

[23]Z. Niu, L. Wang, Y. Niu, B. Hu, M. Zhang, and W. Qin, "Spatiotemporal variations of photosynthetically active radiation and the influencing factors in China from 1961 to 2016," Theor. Appl. Climatol. **137**, 2049–2067 (2019).

[24]A. P. Oliveira, J. F. Escobedo, A. J. Machado, and J. Soares, "Correlation models of diffuse solar-radiation applied to the city of São Paulo, Brazil," Appl. Energy **71**, 59–73 (2002).

[25]J. Soares, A. P. Oliveira, M. Z. Božnar, P. Mlakar, J. F. Escobedo, and A. J. Machado, "Modeling hourly diffuse solar-radiation in the city of São Paulo using a neural-network technique," Appl. Energy **79**, 201–214 (2004).

[26]L. Wong and W. Chow, "Solar radiation model," Appl. Energy **69**, 191–224 (2001).

[27]R. E. Bird and C. Riordan, "Simple solar spectral model for direct and diffuse irradiance on horizontal and tilted planes at the earth's surface for cloudless atmospheres," J. Clim. Appl. Meteorol. **25**(1), 87–97 (1986).

[28]C. Gueymard, *Simple Model for the Atmospheric Radiative Transfer of Sunshine (SMARTS2) Algorithms and Performance Assessment* (Florida Solar Energy Center, 1995), p. 84.

[29]C. Emde, R. Buras-Schnell, A. Kylling, B. Mayer, J. Gasteiger, U. Hamann, J. Kylling, B. Richter, C. Pause, T. Dowling, and L. Bugliaro, "The libRadtran software package for radiative transfer calculations (version 2.0.1)," Geosci. Model Dev. **9**, 1647–1672 (2016).

[30]W. Wandji Nyamsi, P. Blanc, J. A. Augustine, A. Arola, and L. Wald, "A new clear-sky method for assessing photosynthetically active radiation at the surface level," Atmosphere **10**, 219 (2019).

[31]C. Thomas, S. Dorling, W. Wandji Nyamsi, L. Wald, S. Rubino, L. Saboret, M. Trolliet, and E. Wey, "Assessment of five different methods for the estimation of surface photosynthetically active radiation from satellite imagery at three sites—application to the monitoring of indoor soft fruit crops in southern UK," Adv. Sci. Res. **16**, 229–240 (2019).

[32]I. Foyo-Moreno, I. Alados, and L. Alados-Arboledas, "A new conventional regression model to estimate hourly photosynthetic photon flux density under all sky conditions," Int. J. Climatol. **37**, 1067–1075 (2017).

[33]A. Weiss and J. Norman, "Partitioning solar radiation into direct and diffuse, visible and near-infrared components," Agric. Meteorol. **34**(2-3), 205–213 (1985).

[34]J. C. Kathilankal, T. L. O'Halloran, A. Schmidt, C. V. Hanson, and B. E. Law, "Development of a semi-parametric PAR (Photosynthetically Active Radiation) partitioning model for the United States, version 1.0," Geosci. Model Dev. **7**(5), 2477–2484 (2014).

[35]I. Alados, I. Foyo-Moreno, and L. Alados-Arboledas, "Photosynthetically active radiation: Measurements and modelling," Agric. Meteorol. **78**, 121–131 (1996).

[36]G. Lopez, M. Rubio, M. Martinez, and F. Batlles, "Estimation of hourly global photosynthetically active radiation using artificial neural network models," Agric. Meteorol. **107**, 279–291 (2001).

[37]B. Hu, Y. Wang, and G. Liu, "Spatiotemporal characteristics of photosynthetically active radiation in China," J. Geophys. Res. **112**(D14), D14106, https://doi.org/10.1029/2006JD007965 (2007).

[38]I. Foyo-Moreno, I. Alados, and L. Alados-Arboledas, "A new empirical model to estimate hourly diffuse photosynthetic photon flux density," Atmos. Res. **203**, 189–196 (2018).

[39]P. Trisolino, A. d Sarra, D. Meloni, and G. Pace, "Determination of global and diffuse photosynthetically active radiation from a multifilter shadowband radiometer," Appl. Opt. **55**, 8280 (2016).

[40]W. Su, T. P. Charlock, F. G. Rose, and D. Rutan, "Photosynthetically active radiation from Clouds and the Earth's Radiant Energy System (CERES) products," J. Geophys. Res. **112**, G02022, https://doi.org/10.1029/2006JG000290 (2007).

06 March 2024 18:16:51

© Author(s) 2024

[41]S. Janjai and R. Wattan, "Development of a model for the estimation of photosynthetically active radiation from geostationary satellite data in a tropical environment," Remote Sens. Environ. **115**, 1680–1693 (2011).
[42]D. Hao, G. R. Asrar, Y. Zeng, Q. Zhu, J. Wen, Q. Xiao, and M. Chen, "Estimating hourly land surface downward shortwave and photosynthetically active radiation from DSCOVR/EPIC observations," Remote Sens. Environ. **232**, 111320 (2019).
[43]S. Nwokolo, "A global review of empirical models for estimating photosynthetically active radiation," Trends Renewable Energy **4**(2), 236 (2018).
[44]M. M. A. Noriega Gardea, L. F. Corral Martínez, M. Anguiano Morales, G. Trujillo Schiaffino, and D. P. Salas Peimbert, "Modelling photosynthetically active radiation: A review," Atmósfera **34**, 357 (2020).
[45]X. Yu and X. Guo, "Hourly photosynthetically active radiation estimation in Midwestern United States from artificial neural networks and conventional regressions models," Int. J. Biometeorol. **60**(8), 1247–1259 (2016).
[46]S. Ma Lu, S. Zainali, B. Stridh, A. Avelin, S. Amaducci, M. Colauzzi, and P. Campana, "Photosynthetically active radiation decomposition models for agrivoltaic systems applications," Sol. Energy **244**, 536–549 (2022).
[47]J. González and J. Calbó, "Modelled and measured ratio of PAR to global radiation under cloudless skies," Agric. Meteorol. **110**, 319–325 (2002).
[48]X. Yu, Z. Wu, W. Jiang, and X. Guo, "Predicting daily photosynthetically active radiation from global solar radiation in the Contiguous United States," Energy Convers. Manage. **89**, 71–82 (2015).
[49]T. Akitsu, A. Kume, Y. Hirose, O. Ijima, and K. N. Nasahara, "On the stability of radiometric ratios of photosynthetically active radiation to global solar radiation in Tsukuba, Japan," Agric. Meteorol. **209-210**, 59–68 (2015).
[50]I. Lozano, G. Sánchez-Hernández, J. Guerrero-Rascado, I. Alados, and I. Foyo-Moreno, "Analysis of cloud effects on long-term global and diffuse photosynthetically active radiation at a Mediterranean site," Atmos. Res. **268**, 106010 (2022).
[51]C. P. Jacovides, F. S. Tymvios, D. N. Asimakopoulos, K. M. Theofilou, and S. Pashiardes, "Global photosynthetically active radiation and its relationship with global solar radiation in the Eastern Mediterranean basin," Theor. Appl. Climatol. **74**(3-4), 227–233 (2003).
[52]R. Li, L. Zhao, Y. Ding, S. Wang, G. Ji, Y. Xiao, G. Liu, and L. Sun, "Monthly ratios of PAR to global solar radiation measured at Northern Tibetan Plateau, China," Sol. Energy **84**, 964–973 (2010).
[53]N. D. Proutsos, A. Liakatas, S. G. Alexandris, I. X. Tsiros, D. Tigkas, and G. Halivopoulos, "Atmospheric factors affecting global solar and photosynthetically active radiation relationship in a Mediterranean forest site," Atmosphere **13**, 1207 (2022).
[54]L. Gu, J. D. Fuentes, H. H. Shugart, R. M. Staebler, and T. A. Black, "Responses of net ecosystem exchanges of carbon dioxide to changes in cloudiness: Results from two North American deciduous forests," J. Geophys. Res. **104**(D24), 31421–31434, http://dx.doi.org/10.1029/1999JD901068 (1999).
[55]C. Jacovides, J. Boland, D. Asimakopoulos, and N. Kaltsounides, "Comparing diffuse radiation models with one predictor for partitioning incident PAR radiation into its diffuse component in the eastern Mediterranean basin," Renewable Energy **35**(8), 1820–1827 (2010).
[56]A. J. Oliphant and P. C. Stoy, "An evaluation of semiempirical models for partitioning photosynthetically active radiation into diffuse and direct beam components," J. Geophys. Res.: Biogeosci. **123**(3), 889–901, https://doi.org/10.1002/2017JG004370 (2018).
[57]X. Ren, H. He, L. Zhang, and G. Yu, "Global radiation, photosynthetically active radiation, and the diffuse component dataset of China, 1981–2010," Earth Syst. Sci. Data **10**(3), 1217–1226 (2018).
[58]M. de Blas, A. García-Rodríguez, I. García, and J. L. Torres, "Validation and calibration of models to estimate photosynthetically active radiation considering different time scales and sky conditions," Adv. Space Res. **70**, 1737–1760 (2022).
[59]C. B. Galacho, *Over 1000 visitors experienced cutting-edge agricultural research at AU Viborg* (Aarhus University, 2023).
[60]M. A. A. Mamun, P. Dargusch, D. Wadley, N. A. Zulkarnain, and A. A. Aziz, "A review of research on agrivoltaic systems," Renewable Sustainable Energy Rev. **161**, 112351 (2022).
[61]A. García-Rodríguez, S. García-Rodríguez, M. Díez-Mediavilla, and C. Alonso-Tristán, "Photosynthetic active radiation, solar irradiance and the CIE standard sky classification," Appl. Sci. **10**, 8007 (2020).
[62]D. Yang and J. Boland, "Satellite-augmented diffuse solar radiation separation models," J. Renewable Sustainable Energy **11**(2), 023705 (2019).
[63]B. Ridley, J. Boland, and P. Lauret, "Modelling of diffuse solar fraction with multiple predictors," Renewable Energy **35**, 478–483 (2010).
[64]H. Lu, Z. Qin, S. Lin, X. Chen, B. Chen, B. He, J. Wei, and W. Yuan, "Large influence of atmospheric vapor pressure deficit on ecosystem production efficiency," Nat. Commun. **13**, 1653 (2022).
[65]M. Yamashita and M. Yoshimura, "Estimation of global and diffuse photosynthetic photon flux density under various sky conditions using ground-based whole-sky images," Remote Sens. **11**, 932 (2019).
[66]A. R. Starke, L. F. Lemos, J. Boland, J. M. Cardemil, and S. Colle, "Resolution of the cloud enhancement problem for one-minute diffuse radiation prediction," Renewable Energy **125**, 472–484 (2018).
[67]C. Spitters, H. Toussaint, and J. Goudriaan, "Separating the diffuse and direct component of global radiation and its implications for modeling canopy photosynthesis. Part I. Components of incoming radiation," Agric. Meteorol. **38**(1-3), 217–229 (1986).
[68]P. Ineichen, "A broadband simplified version of the Solis clear sky model," Sol. Energy **82**, 758–762 (2008).
[69]F. Kasten and A. T. Young, "Revised optical air mass tables and approximation formula," Appl. Opt. **28**, 4735 (1989).
[70]R. G. Allen, I. A. Walter, R. L. Elliott, T. A. Howell, D. Itenfisu, M. E. Jensen, R. L. Snyder, and Technical Committee on Standardization of Reference Evapotranspiration, *The ASCE Standardized Reference Evapotranspiration Equation* (American Society of Civil Engineers, Reston, 2005).
[71]MathWorks, "fitnlm" (2023).
[72]T. Gneiting, "Making and evaluating point forecasts," J. Am. Stat. Assoc. **106**, 746–762 (2011).
[73]D. Yang, S. Alessandrini, J. Antonanzas, F. Antonanzas-Torres, V. Badescu, H. G. Beyer, R. Blaga, J. Boland, J. M. Bright, C. F. Coimbra, M. David, z Frimane, C. A. Gueymard, T. Hong, M. J. Kay, S. Killinger, J. Kleissl, P. Lauret, E. Lorenz, D. van der Meer, M. Paulescu, R. Perez, O. Perpiñán-Lamigueiro, I. M. Peters, G. Reikard, D. Renné, Y.-M. Saint-Drenan, Y. Shuai, R. Urraca, H. Verbois, F. Vignola, C. Voyant, and J. Zhang, "Verification of deterministic solar forecasts," Sol. Energy **210**, 20–37 (2020).
[74]D. Yang and J. Kleissl, "Summarizing ensemble NWP forecasts for grid operators: Consistency, elicitability, and economic value," Int. J. Forecast. **39**, 1640 (2022).
[75]D. Erbs, S. Klein, and J. Duffie, "Estimation of the diffuse radiation fraction for hourly, daily and monthly-average global radiation," Sol. Energy **28**, 293–302 (1982).
[76]W. F. Holmgren, C. W. Hansen, and M. A. Mikofski, "pvlib python: A python package for modeling solar energy systems," J. Open Source Software **3**, 884 (2018).
[77]ICOS Sweden Coordination Office, "ICOS Sweden" (2022).
[78]N. Engerer, "Minute resolution estimates of the diffuse fraction of global irradiance for southeastern Australia," Sol. Energy **116**, 215–237 (2015).
[79]C. A. Gueymard and J. A. Ruiz-Arias, "Extensive worldwide validation and climate sensitivity analysis of direct irradiance predictions from 1min global irradiance," Sol. Energy **128**, 1–30 (2016).
[80]D. Doelling, *CERES Level 3 SYN1deg-1Hour Terra-Aqua-MODIS HDF4 file - Edition 4A* (Atmospheric Science Data Center, 2017).
[81]ECMWF, "CAMS-AOD" (2022).
[82]H. Hersbach, B. Bell, P. Berrisford, G. Biavati, A. Horány, J. Muñoz Sabater, J. Nicolas, C. Peubey, R. Radu, I. Rozum, D. Schepers, A. Simmons, C. Soci, D. Dee, and J.-N. Thépaut, "ERA5 hourly data on single levels from 1940 to present" (ECMWF, 2023).
[83]A. W. T. Barenbrug, *Psychrometry and Psychrometric Charts*, 3rd ed. (Chamber of Mines of South Africa, Johannesburg, 1974).
[84]A. Carrara, P. Kolari, M. O. De Beeck, N. Arriga, D. Berveiller, S. Dengel, A. Ibrom, L. Merbold, C. Rebmann, S. Sabbatini, P. Serrano-Ortíz, and S. C. Biraud, "Radiation measurements at ICOS ecosystem stations," Int. Agrophys. **32**, 589–605 (2018).
[85]GADM, "GADM" (2022).

06 March 2024 18:16:51

© Author(s) 2024

[86]R. A. I. Wilcke, E. Kjellström, C. Lin, D. Matei, A. Moberg, and E. Tyrlis, "The extremely warm summer of 2018 in Sweden—set in a historical context," Earth Syst. Dyn. **11**, 1107–1121 (2020).
[87]J. Räisänen, "Energetics of interannual temperature variability," Clim. Dyn. **52**, 3139–3156 (2019).
[88]V. A. Sinclair, J. Mikkola, M. Rantanen, and J. Räisänen, "The summer 2018 heatwave in Finland," Weather **74**, 403–409 (2019).
[89]P. Trisolino, A. di Sarra, F. Anello, C. Bommarito, T. Di Iorio, D. Meloni, F. Monteleone, G. Pace, S. Piacentino, and D. Sferlazzo, "A long-term time series of global and diffuse photosynthetically active radiation in the Mediterranean: Interannual variability and cloud effects," Atmos. Chem. Phys. **18**, 7985–8000 (2018).
[90]J. Chen, M. Shen, and T. Kato, "Diurnal and seasonal variations in light-use efficiency in an alpine meadow ecosystem: Causes and implications for remote sensing," J. Plant Ecol. **2**, 173–185 (2009).
[91]J. A. Duffie and W. A. Beckman, *Solar Engineering of Thermal Processes*, 4th ed. (John Wiley, Hoboken, 2013).
[92]C. A. Gueymard, "Revised composite extraterrestrial spectrum based on recent solar irradiance observations," Sol. Energy **169**, 434–440 (2018).
[93]J. W. Spencer, "Fourier series representation of the position of the sun," Search **2**(5), 172 (1971).
[94]D. Koblick, *Vectorized solar Azimuth and elevation estimation* (MATLAB Central File Exchange, 2021).
[95]US Department of Commerce, "ESRL Global Monitoring Laboratory - Global Radiation and Aerosols" (2021).
[96]B. A. Wielicki, B. R. Barkstrom, E. F. Harrison, R. B. Lee, G. Louis Smith, and J. E. Cooper, "Clouds and the Earth's Radiant Energy System (CERES): An earth observing system experiment," Bull. Am. Meteorol. Soc. **77**, 853–868 (1996).
[97]Delta-T Devices, "BF5 Sunshine Sensor - Pyranometer - Solar Radiation" (2022).
[98]H. A. Herrmann, J.-M. Schwartz, and G. N. Johnson, "From empirical to theoretical models of light response curves - linking photosynthetic and metabolic acclimation," Photosynth. Res. **145**, 5–14 (2020).
[99]C. Schaaf and Z. Wang, *MODIS/Terra+Aqua BRDF/Albedo Model Parameters Daily L3 Global - 500m V061* (Level-1 and Atmosphere Archive and Distribution System, 2021).
[100]G. M. Yagli, D. Yang, O. Gandhi, and D. Srinivasan, "Can we justify producing univariate machine-learning forecasts with satellite-derived solar irradiance?," Appl. Energy **259**, 114122 (2020).
[101]S. Zainali, S. Ma Lu, B. Stridh, A. Avelin, S. Amaducci, M. Colauzzi, and P. E. Campana, "Direct and diffuse shading factors modelling for the most representative agrivoltaic system layouts," Appl. Energy **339**, 120981 (2023).
[102]R. Li, D. Wang, and S. Liang, "Comprehensive assessment of five global daily downward shortwave radiation satellite products," Sci. Remote Sens. **4**, 100028 (2021).
[103]Google Maps, "Kärrbo Prästgård" (2023).
[104]J. M. Bright and N. A. Engerer, "Engerer2: Global re-parameterisation, update, and validation of an irradiance separation model at different temporal resolutions," J. Renewable Sustainable Energy **11**(3), 033701 (2019).

06 March 2024 18:16:51

© Author(s) 2024